

24 Modeling of Quasi-One-Dimensional Carbon Nanostructures with Density Functional Theory

Veronica Barone¹ · Oded Hod² · Juan E. Peralta¹

¹Department of Physics, Central Michigan University, Mount Pleasant, Michigan, USA

²Department of Chemical Physics, School of Chemistry, The Sackler Faculty of Exact Sciences, Tel Aviv University, Tel Aviv, Israel

<i>Density Functional Theory with Periodic Boundary Conditions</i>	903
<i>Structure–Property Relations in Single-Walled Carbon Nanotubes and Graphene</i>	
<i>Nanoribbons</i>	905
Single-Walled Carbon Nanotubes	905
Graphene Nanoribbons	906
<i>Modeling the Optical Spectrum of Single-Walled Carbon Nanotubes and Graphene</i>	
<i>Nanoribbons</i>	912
Single-Walled Carbon Nanotubes	912
Graphene Nanoribbons	915
<i>Chemistry at the Edges of Graphene</i>	916
<i>Finite Size Effects in Low-Dimensional Graphitic Materials</i>	
Quantum Confinement in Graphitic Systems	918
Edge Effects in Graphitic Systems	921
<i>Electromechanical Properties of One-Dimensional Graphitic Structures</i>	
Carbon Nanotubes in NEMS Applications	926
Graphene Nanoribbons in NEMS Applications	930

Concluding Remarks 932

Acknowledgments 932

References 932

Abstract: The purpose of this chapter is to describe and review examples of how theoretical investigations can be applied to elucidate the behavior of carbon nanostructures and to understand the physical mechanisms taking place at the molecular level. We will place a special emphasis in theoretical works utilizing density functional theory. We assume that the reader is familiar with the basics of density functional theory as well as the electronic properties of single-walled carbon nanotubes and graphene nanoribbons (GNRs). We do not intend to present an extensive review; instead, we focus on several examples to illustrate the powerful predictive capabilities of current computational approaches.

Density Functional Theory with Periodic Boundary Conditions

The focus of this chapter is on carbon structures that are elongated, predominantly one-dimensional systems. For most modeling purposes, these structures can be considered as periodic in one dimension. There are many software packages either free or commercially available to perform density functional theory (DFT) calculations using periodic boundary conditions. In fact, these type of calculations are routine in condensed matter physics and became very popular recently in the quantum chemistry community. One of the most widely used approaches for DFT calculations with periodic boundary conditions is the combination of the local density approximation (LDA) or the generalized gradient approximation (GGA) and plane waves. This approach usually involves only valence electrons, while the effect of core electrons is represented with pseudopotentials. Many modern pseudopotential calculations use ultrasoft pseudopotentials, which were first developed by Vanderbilt in the early 1990s (Vanderbilt 1990). Full-potential all-electron calculations can also be performed using plane waves, although they are somewhat computationally expensive for routine calculations. On the other hand, another class of software packages employ localized basis functions such as Gaussians. These basis functions allow not only an all-electron treatment of the system but also present the flexibility of pseudopotential calculations when heavy atoms are involved. In most cases, dealing with systems involving first- and second-row elements in an all-electron fashion can be routinely done. Another advantage of localized basis functions is that periodic boundary conditions can be explicitly imposed in either one, two, or three dimensions, in contrast to plane waves, which are naturally periodic in three dimensions and therefore approaches such as the super-cell are commonly used to reduce the dimensionality from three to two or one at the price of increasing the computational cost. The main advantage of plane waves over Gaussian basis functions is that the basis set convergence is more controlled. The basis set convergence of Gaussian-type orbitals is well known for molecules and there are tens of available basis sets developed for different purposes (see for instance the EMSL library Feller 1996, 2007). However, the basis set convergence of Gaussian functions is less known for periodic systems, especially for properties like the bandgap. Another disadvantage of Gaussians is that available basis for molecular systems cannot always be straightforwardly employed in periodic boundary conditions calculations due to linear dependencies that occur in periodic structures, limiting in practice the use of large exponents (Gruneich and Hess 1998).

When using localized functions, in general, the basis set needs to be carefully chosen in order to obtain sensible results. It is important to point out that using either localized basis or plane waves, different properties can have different basis set convergence behavior, and the fact that one property such as the energy is converged (within a given criterion) does not imply that

all properties are converged. In single-walled carbon nanotubes (SWNTs), for instance, the choice of the Gaussian basis set does not seem to have a significant impact on the bandgap. In ► [Table 24-1](#), we show the bandgap (obtained as Kohn–Sham band energy differences) of the (10,0) SWNT calculated with different functionals and standard Gaussian basis sets. The initial SWNT geometry was obtained with the *Tubegen* program (Frey and Doren 2005) and then relaxed using the different functionals and basis sets indicated in each column. For each optimized structure, we calculate the bandgap of the system with the different functionals and basis sets. As shown in ► [Table 24-1](#), the bandgap does not depend significantly on the level of theory utilized for the geometry optimization, or the basis set. ► [Table 24-1](#) illustrates, however, the dependence of the bandgap upon the choice of the exchange–correlation (XC) functional. This shows that for SWNTs, the choice of the XC functional has a larger impact on the calculated bandgap and related properties.

There are several options available in DFT software packages for the choice of the approximate XC functional. The most widely used XC functionals depend either on the electronic density (local[σ -spin] density approximation or L[S]DA) or on the electronic density and its gradient (generalized gradient approximation or GGA). For example, in ► [Table 24-1](#) we employ the combination of Dirac exchange and the parameterization of Vosko et al. (1980) for correlation in the LSDA functional and the GGA functional of Perdew, Burke, and Ernzerhof (PBE) (1996). Comparing with available experimental data, these families of functionals usually perform well for structural properties but have some deficiencies for energetics and electronic properties. Other type of approximate XC functionals include an orbital dependency either through quantities such as the kinetic energy density or Hartree–Fock (HF) type of exchange (for a thorough review, see Kümmel and Kronik 2008). Examples of orbital-dependent functionals are the meta-GGA TPSS (Tao et al. 2003), or the hybrid functionals PBE0 (Adamo and Barone 1999; Ernzerhof and Scuseria 1999; Perdew et al. 1997) (also known as PBEh), and B3LYP(Becke 1993). These type of functionals generally show some improvement over the LSDA and GGA but are computationally more demanding. In particular, due to the nature of the HF approximation, hybrid functionals in extended systems can be extremely demanding for metallic and small bandgap systems (Paier et al. 2007). An alternative to standard hybrid functionals for extended systems are the short-range hybrid functionals such as HSE (Heyd et al. 2003, 2006). These functionals truncate the long-range tail of the electron–electron interaction in the exchange contribution to the electronic energy. In this way, the remaining (short-range) part of the HF exchange can be efficiently evaluated (Adamson et al. 1996, 1999). It has been shown that this truncation has little effect on the properties of finite systems and at the same

► **Table 24-1**

Bandgaps (in eV) for the (10,0) SWNT obtained with different functionals (LDA, PBE, and HSE, shown row-wise) and basis sets (3-21G, 3-21G*, and 6-31G*, shown column-wise).

	LDA optimized			PBE optimized			HSE optimized		
	3-21G	3-21G*	6-31G*	3-21G	3-21G*	6-31G*	3-21G	3-21G*	6-31G*
LDA	0.79	0.79	0.78	0.77	0.77	0.76	0.79	0.79	0.77
PBE	0.80	0.80	0.79	0.78	0.78	0.76	0.79	0.79	0.78
HSE	1.00	1.00	0.98	0.97	0.97	0.96	0.99	0.99	0.98

The structure was optimized using the functional and basis set indicated in each column. Calculations were performed with the Gaussian development program (Frisch et al. 2006)

time provides an efficient route for hybrid DFT calculations in extended systems (Heyd and Scuseria 2004).

Most commonly available functionals, either derived from nonempirical grounds or using fitting procedures, are meant to approximate only the electronic ground state, and not excited states. Moreover, although in “static” DFT, Kohn–Sham eigenvalues are often used to evaluate the energy bandgap, there is no formal justification for this: The formal theoretical framework is provided by time-dependent DFT (Runge and Gross 1984). For a review, see Onida et al. (2002). Therefore, the evaluation of the energy bandgaps and related properties from DFT calculations needs to be carried out with care. From a pragmatic viewpoint, Kohn–Sham eigenvalues are often used to distinguish between metals and semiconductors and to estimate excitation energies. LSDA and GGA Kohn–Sham gaps usually underestimate experimental data and sometimes small-gap semiconductors are erroneously predicted to be metallic. Kohn–Sham gaps from hybrid functional calculations, on the other hand are, in general, in better agreement with experimental gaps (Barone et al. 2005a, b; Heyd et al. 2005; Kümmel and Kronik 2008; Peralta et al. 2006), although they tend to overestimate, in general, the available experimental data. Short-range hybrid functionals improve upon regular hybrids and provide good agreement with experiments and more sophisticated many-electron approaches (Barone et al. 2005b; Batista et al. 2006).

Structure–Property Relations in Single-Walled Carbon Nanotubes and Graphene Nanoribbons

Single-Walled Carbon Nanotubes

Carbon nanotubes are one of the most fascinating carbon nanostructures. Although soon after the discovery of fullerenes in 1985 (Kroto et al. 1985) there were many speculations about the possibility of synthesizing long and narrow graphitic cage-like structures, the synthesis of the first carbon nanotubes was reported by Iijima in 1991. After that seminal work, several new routes toward the synthesis of single- and multi-walled carbon nanotubes were developed.

The electronic properties of SWNT were first studied within the so-called zone-folding scheme (ZF) (Hamada et al. 1992; Saito et al. 1992, 1998). This scheme is based on the tight-binding (TB) approximation for the two-dimensional honeycomb lattice and the subsequent quantization of the wave vector associated with the radial direction of the nanotube. In this framework, the electronic structure of SWNTs is determined by the allowed values of the quantized wave vector. Within this approach, each nanotube, characterized by the indices (n, m) , can be either metallic if $(2n + m)/3 = k$, with k integer, or semiconducting for k non-integer (with a bandgap that depends on the inverse diameter, $1/d$). This versatility in the electronic behavior, that depends *only* on the geometric structure of the tubes, ignited a large amount of experimental and theoretical efforts with the promise of novel technological applications based on these unique nanostructured materials.

In 1998, Tang et al. produced SWNTs grown in zeolite channels with diameters of about 4 Å (Tang et al. 1998). From the optical spectrum and the possible diameter distributions, these tubes were identified as the (3,3), (4,2), and (5,0) (Li et al. 2001). In 2004, the thinnest SWNTs, with diameters of about 3 Å were grown inside multi-walled nanotubes. Because of the small diameter, the possible (n, m) indices of these narrow SWNT were predicted to be (2,2), (4,0),

and (3,1) (Zhao et al. 2004). DFT calculations pointed out the importance of curvature effects, especially for narrower nanotubes which present a significant σ - π hybridization not accounted for in the ZF scheme (Blase et al. 1994; Gülseren et al. 2002; Mintmire et al. 1992; Reich et al. 2002). Although the ZF scheme works reasonably well for the average diameter SWNT of about 10 Å, several studies confirmed the profound effect of the σ - π hybridization in small diameter SWNT on their electronic properties.

DFT calculations have shown that the zigzag (5,0) SWNT, which should be a semiconductor according to the zone-folding scheme, is indeed metallic (Barone and Scuseria 2004; Cabria et al. 2003; Li et al. 2001; Liu and Chan 2002; Machón et al. 2002; Springborg and Satpathy 1994). The same holds true for the zigzag (4,0) SWNT (Barone and Scuseria 2004; Cabria et al. 2003). Although it is tempting to assume that narrower tubes tend to be metallic due to the σ - π hybridization, it has been shown that the narrowest chiral tubes (4,3) and (3,1) present the largest bandgaps of all SWNTs (1.7 and 1.3 eV, respectively, obtained with the HSE functional) (Barone and Scuseria 2004). Due to curvature effects, most narrow semiconducting SWNTs become indirect gap semiconductors and largely deviate from the ZF $1/d$ predictions.

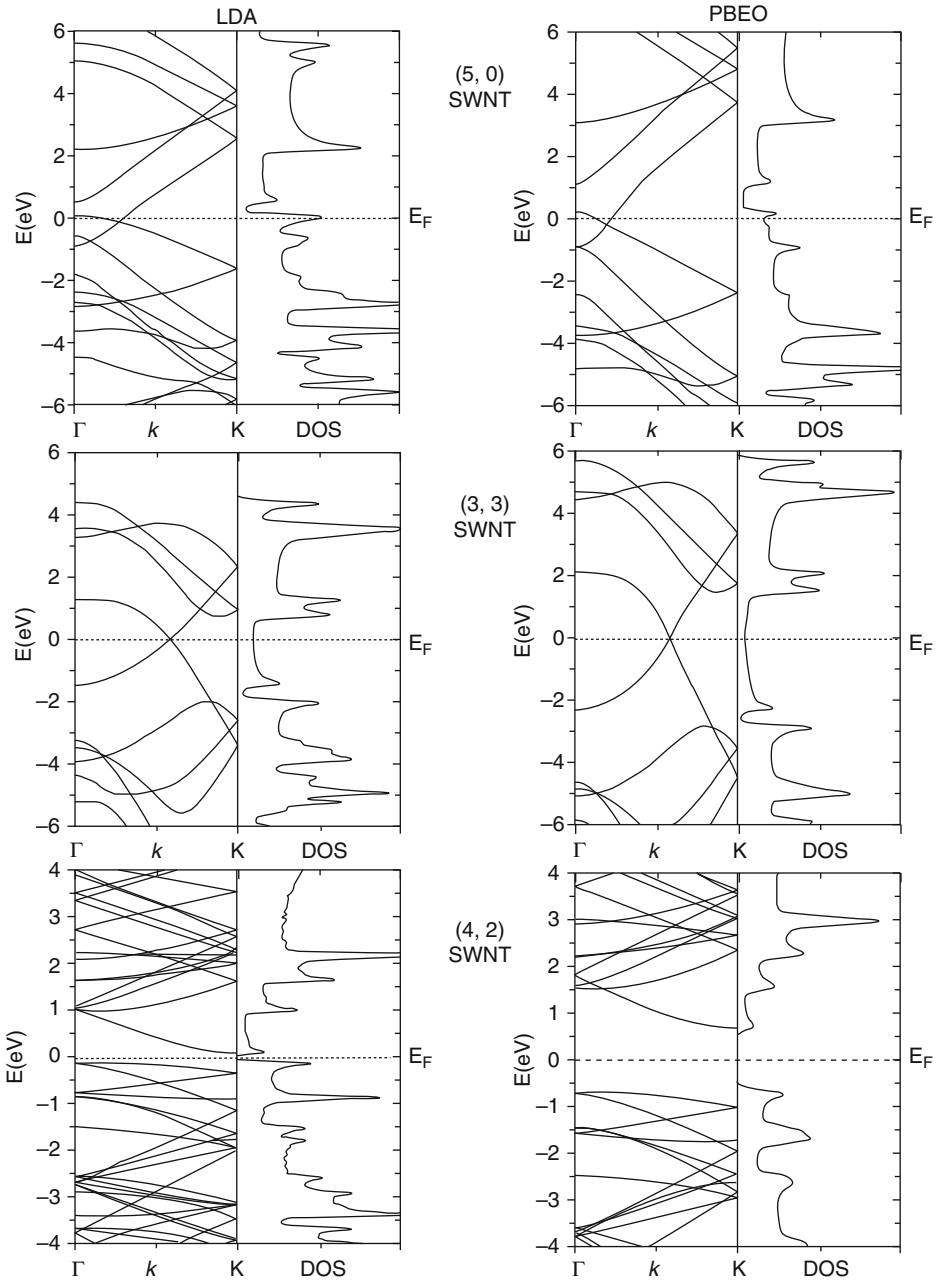
On the modeling side, we note that the calculated electronic properties of narrow nanotubes strongly depend on the exchange-correlation functional used. In [Fig. 24-1](#) we show the band structure and density of states (DOS) for the three narrow (5,0), (3,3), and (4,2) nanotubes obtained with LDA and the hybrid PBE0 functionals. The largest differences are found for the chiral semiconducting tube for which PBE0 predicts a bandgap as large as 1.36 eV. However, as we show in [section “Modeling the Optical Spectrum of Single-Walled Carbon Nanotubes and Graphene Nanoribbons,”](#) while the bandgap of SWNTs is largely underestimated by LSDA, it is also significantly overestimated by PBE0.

Graphene Nanoribbons

Graphene, a single layer of graphite, has attracted a lot of attention since 2004 when it was isolated for the first time as a stand-alone two-dimensional all-carbon network (Novoselov et al. 2004). Since then, major accomplishments in their production have been achieved and now, lower dimensional graphene derivatives are routinely created in the lab (Berger et al. 2006; Cai et al. 2010; Han et al. 2007; Ritter and Lyding 2009; Wang et al. 2008; Yang et al. 2008). Recent studies point to graphene and its derivatives as one of the most promising materials for technological applications ranging from spintronic devices to energy storage media (Bhardwaj et al. 2010; Son et al. 2006b).

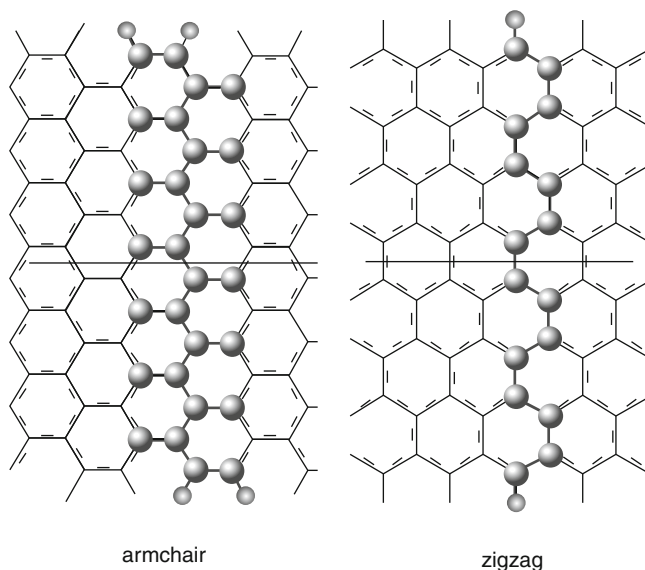
By cutting a quasi-one-dimensional structure out of a two-dimensional graphene sheet, it is possible to obtain a flat structure usually referred to as a graphene nanoribbon (GNR). These ribbons can also be thought of as unwrapped nanotubes of a given chirality. In [Fig. 24-2](#) we present a scheme of the two extreme crystallographic orientations of the GNRs axis: armchair (AGNR) and zigzag (ZGNR). Dangling bonds at the edges are usually passivated with hydrogen atoms for the purpose of performing computational studies as it is very difficult to experimentally determine the chemical nature of the edges.

One of the earliest theoretical investigations of the electronic properties of these materials was reported by Fujita et al. (1996). In that work, the authors report striking differences between armchair and zigzag GNRs. Most notably, the authors found that magnetism can



■ Fig. 24-1

Band structure and electronic density of states for the (5,0), (3,3), and (4,2) SWNT. (a) Obtained at the LDA/6-31G* level. (b) Obtained at the PBE0/6-31G* level

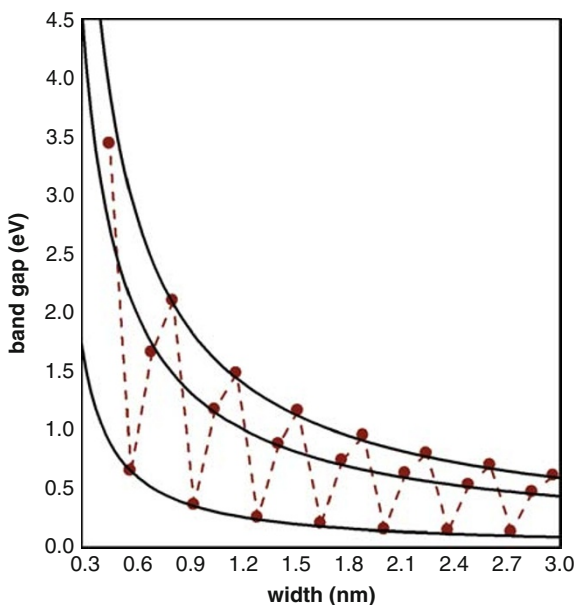


■ Fig. 24-2

Schematic representation of the fundamental cell of an armchair and a zigzag graphene nanoribbon. The horizontal line represents the translational vector

arise in nanometer-scale graphitic fragments in the zigzag configuration due to the appearance of localized edge states. According to TB calculations these edge states are manifested as flat bands near the Fermi energy in the band structure of the system. We will return to the case of ZGNRs later in this section. AGNRs do not present such edge states. Instead, the bandgap of these ribbons is predicted to vary with a three fold periodicity as a function of their width, changing from metallic to semiconducting as one consecutively increases their width (Ezawa 2006). When electronic correlation effects are taken into account via DFT, similar bandgap oscillations appear. Nevertheless, a major difference is identified. While in the TB calculations, at certain widths, AGNRs appear to become metallic, DFT calculations predict all AGNRs to be semiconducting (Barone et al. 2006; Son et al. 2006a). In ● Fig. 24-3, we present DFT results for the bandgap of armchair ribbons as a function of their width. As shown in this figure, ultra-narrow graphene nanoribbons with widths up to 1 nm present the largest bandgaps in the range of 1–3 eV. For the range of widths covered by the DFT calculations (up to 3 nm), no significant quenching of the energy gap oscillations is observed (Barone et al. 2006). However, GNRs are expected to reach the graphene limit of zero bandgap for sufficiently large widths.

We note that the armchair GNRs bandgaps presented in ● Fig. 24-3 can be separated into three groups, namely, the points forming the envelope of the maxima of the oscillations, those forming the envelope of the minima of the oscillations, and the remaining intermediate points. It is possible then to extrapolate the behavior of each of these subgroups independently to larger widths. Such an extrapolation can be performed using an inverse power law with two fitting parameters (Barone et al. 2006). This simple rule presents the correct asymptotic behavior and provides qualitative information on the electronic structure of ribbons beyond the range of



■ Fig. 24-3

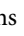
Bandgap of H-terminated armchair GNRs as a function of the width obtained with the HSE functional (Reprinted (Adapted) with permission from Barone et al. (2006). © (2006) American Chemical Society)

widths studied by first-principles calculations. From these calculations, it is shown that in order to obtain an AGNR with a bandgap comparable to that of Ge (0.67 eV) or InN (0.7 eV), it will be necessary to go to a range of widths between 2 and 3 nm. If a larger band gap material is needed (like Si, 1.14 eV, or GaAs, 1.43 eV), the width of the AGNR must be reduced to as low as 1–2 nm. The extrapolation to wider ribbons also shows that an AGNR of about 8 nm will present a bandgap smaller than 0.2 eV. It is interesting to note that when the first DFT calculations on these systems were carried out, it seemed impossible to produce nanoribbons as narrow as a few nanometers. Only 3 years later, the fabrication and electrical measurement of nanoribbons with widths down to a few nanometers are performed routinely in many laboratories around the world (Wang et al. 2008; Yang et al. 2008; Berger et al. 2006; Cai et al. 2010; Han et al. 2007; Ritter and Lyding 2009).

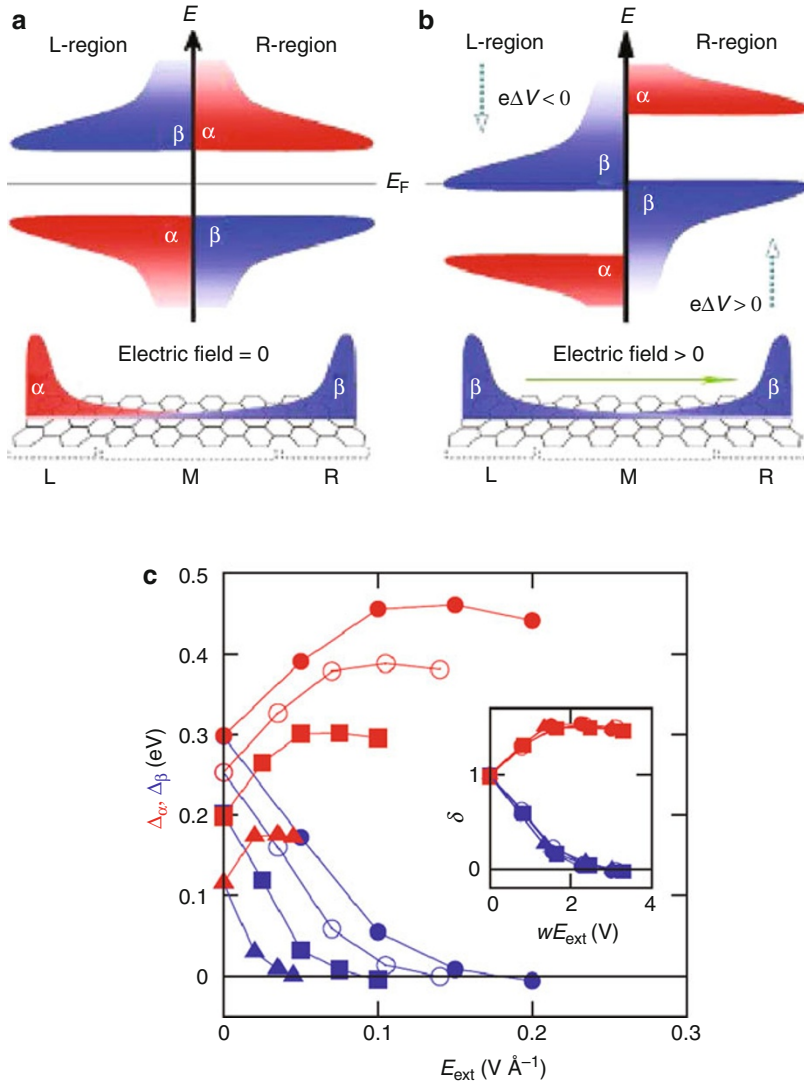
Experimentally, it has been demonstrated that the energy gap in graphene nanoribbons can be tuned during fabrication and that the energy gap scales inversely with the ribbon width (Chen et al. 2007; Han et al. 2007). Suspended GNRs with widths below 10 nm have been synthesized by a chemical route (Wang et al. 2008). However, the uncontrollable character of these methods restrict the quality of the GNR's edges and consequently limit their applications. Novel, organic synthetic protocols leading to graphene type molecules with different sizes have been presented recently (Yang et al. 2008; Cai et al. 2010). This route should provide perfect edged narrow graphene nanoribbons with widths up to 12 nm.

In zigzag graphene nanoribbons, quantum confinement is accompanied by the existence of pronounced edge states localized around the zigzag edges. As mentioned before, the existence of these edge states have been suggested theoretically more than a decade ago (Fujita et al. 1996; Klein 1994; Kobayashi 1993; Nakada et al. 1996; Tanaka et al. 1987). Recently, such states along the zigzag edges of graphite have been experimentally observed (Kobayashi et al. 2005, 2006; Niimi et al. 2005). One of the most interesting characteristics of these edge states in graphite is their predicted magnetic character (Fujita et al. 1996; Kusakabe and Maruyama 2003; Son et al. 2006a; Wakabayashi et al. 1999). Early theoretical predictions of graphene edge states were based on TB and Hubbard models (Fujita et al. 1996; Nakada et al. 1996; Tanaka et al. 1987), Huckel theory (Klein 1994), and the DV- $X\alpha$ method (Kobayashi 1993; Tsukada et al. 1983). A more chemically oriented interpretation of the structure and electronic character of the different edges has recently been given using Clar's sextet theory, a well-known tool for the study of aromaticity in organic materials (Balaban and Klein 2009; Baldoni et al. 2008; Wassmann et al. 2008).

The magnetic character carried by the zigzag edge states has a dominant effect on the electronic structure of the system. If one views a ZGNR as unrolling an armchair SWNT, one would naively expect both systems to have similar electronic character while replacing the symmetry of a "particle in a ring" type of boundary conditions with that of a "particle in a box." Therefore, since all armchair SWNTs are metallic in nature, it can be assumed that all ZGNRs would be metallic as well. When performing spin-restricted DFT calculations, this indeed turns out to be the case (Son et al. 2006b). Nevertheless, if the spin degree of freedom is taken into account via the unrestricted DFT scheme, the spin-polarized character of the electronic ground state of the ZGNR is revealed (Son et al. 2006b). Here, the electronic edge state on one zigzag edge has one spin flavor while the corresponding state on the other zigzag edge has the opposite spin flavor. This antiparallel edge spin alignment is a direct consequence of the antiferromagnetic coupling of spins on adjacent sites within the hexagonal carbon lattice. In contrast to the case of the metallic armchair SWNTs, the magnetic ground state exhibits a finite bandgap, and therefore, all ZGNRs become semiconducting (Son et al. 2006b). This is an excellent example showing how edge states may dominate the electronic character of the system.

The existence of such spin-polarized edge states opens a venue for controlling the electronic properties of GNRs. One possible scheme was recently suggested where an in-plane electric field, applied perpendicular to the axis of the ribbon, drives the system into a half-metallic state (Son et al. 2006b). Due to the field-induced charge separation, a local gating with opposite charge polarization occurs at the edges of the ribbons. This in turn, shifts the local DOS at both edges with respect to one another thus increasing the bandgap of electrons with one spin flavor and reducing the bandgap of the opposite spins (see  Fig. 24-4). By changing the intensity of the applied electric field, one can control the ratio of the bandgaps of the two spin components up to a point where the bandgap of one spin flavor completely vanishes while the other spin flavor presents a large bandgap. A system in such a half-metallic state may serve as a perfect spin filter in nanospintronic devices.

The half-metallic behavior exhibited by zigzag ribbons under an external electric field was first obtained using the LSDA functional. Shortly after, calculations in a large cluster model of a zigzag GNR performed using the hybrid B3LYP challenged those findings arguing that the inclusion of HF exchange prevents the half-metallic behavior (Rudberg et al. 2007). However, Kan et al. (2007) and Hod et al. (2007a) independently found half-metallicity in periodic zigzag nanoribbons using the B3LYP and HSE functionals, respectively.



■ Fig. 24-4

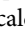
(a) Schematic density of states diagram of the electronic states of a zigzag GNR in the absence of an applied electric field. (b) Schematic density of states diagram in the presence of a transverse electric field. The electrostatic potential on the *left edge* is lowered, whereas the one on the *right edge* is raised. (c) Dependence of half-metallicity on system size. Red denotes the bandgap of α -spin, and blue the gap of β -spin as function of E_{ext} for the 8-GNR (filled circles), 11-GNR (open circles), 16-GNR (squares), and 32-GNR (triangles). The rescaled gaps for the various widths collapse to a single function as shown in the inset (Reprinted with permission from Macmillan Publishers Ltd: Nature (Son et al. 2006b), © (2006))

Modeling the Optical Spectrum of Single-Walled Carbon Nanotubes and Graphene Nanoribbons

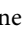
Single-Walled Carbon Nanotubes

Characterization methods for single-walled carbon nanotubes based on optical absorption have attracted much attention during the past few years. Experiments based on photoluminescence (Bachilo et al. 2002; Weisman and Bachilo 2003), resonant Raman spectroscopy (Fantini et al. 2004; Telg et al. 2004), and Rayleigh scattering (Sfeir et al. 2006) have been reported in which optical transitions are obtained as fingerprints of a certain (n,m) SWNT. Optical transitions were first studied theoretically within the tight-binding approach considering the excitations as inter-band transitions. Within this framework, the optical spectra is generally obtained by utilizing the random-phase approximation (RPA) for the imaginary part of the dielectric function ϵ (for a review, see Onida et al. 2002)

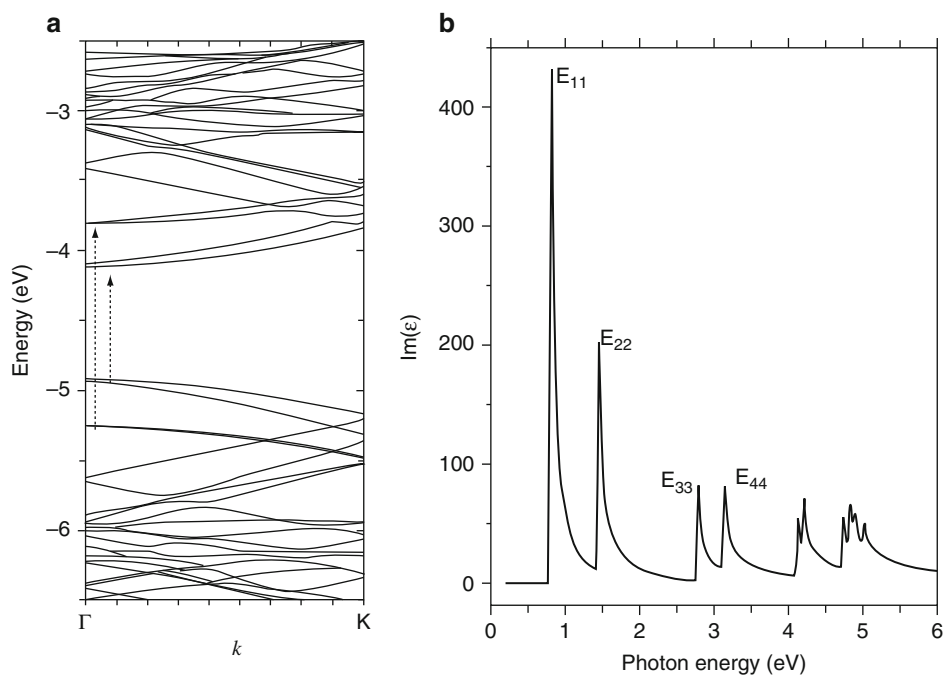
$$\text{Im}(\epsilon) = \frac{1}{\omega^2} \sum_{\mathbf{k}} \sum_{o,u} \left| \langle \psi_o^{\mathbf{k}} | \mathbf{p} | \psi_u^{\mathbf{k}} \rangle \right|^2 \delta(\epsilon_o^{\mathbf{k}} - \epsilon_u^{\mathbf{k}} - \omega), \quad (24.1)$$

where \mathbf{p} is the linear momentum operator and the indices o and u stand for occupied and unoccupied Bloch orbitals, respectively. An example of the band structure and optical spectrum for a semiconducting tube obtained from DFT calculations is shown in  Fig. 24-5. Allowed optical transitions, marked with arrows in the band structure of panel (a), produce a peak in the optical spectrum (panel (b)). Within the RPA the first-order optical transition corresponds to the fundamental gap of the semiconducting SWNT (generally dipole-allowed).

The relation between the optical transitions and the diameter of the nanotubes (Kataura plot) (Kataura et al. 1999) was used as a useful guide for experimentalists in characterizing nanotubes samples. However, Kataura plots based on conventional TB calculations present serious limitations (Bachilo et al. 2002). DFT calculations utilizing local and semi-local functionals are well known to underestimate the bandgap of semiconductors significantly. This holds also true for higher order optical transitions. Hybrid functionals have been shown to improve significantly the description of the bandgap in semiconducting materials (Heyd and Scuseria 2004; Heyd et al. 2005). In the specific case of semiconducting nanotubes, commonly employed hybrid functionals, like B3LYP or PBE0 significantly overestimate the bandgap (Barone et al. 2005b).

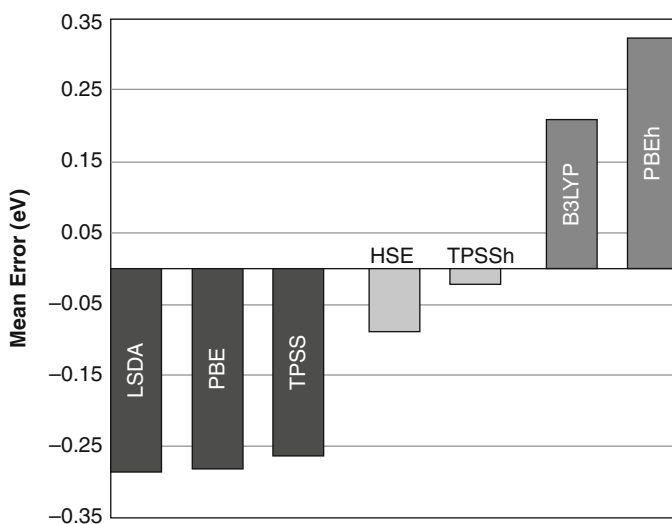
Despite the excitonic character of optical transitions in SWNTs (Spataru et al. 2004), the hybrid meta-GGA TPSS and the screened-exchange hybrid HSE provide excellent agreement with experiments for the optical gap (Barone et al. 2005b) as depicted in  Fig. 24-6 where the mean error for the first-order optical transition with respect to experimental values in a set of ten semiconducting nanotubes is shown. It is worth pointing out, however, that DFT-based approaches cannot predict the strength of exciton binding energies due to the mean-field nature of the approximation.

First-principles calculations including electron–electron interactions beyond the mean field theory have shown the excitonic character of optical transitions in SWNTs with large exciton binding energies (of up to 1 eV for the (8,0) SWNT) (Spataru et al. 2004). These predictions have been corroborated by experiments (Shaver et al. 2007; Wang et al. 2005). Unfortunately, these calculations are too demanding for routine calculations in large diameter tubes, and unlikely to be practical to study the effect of defects and functionalization.



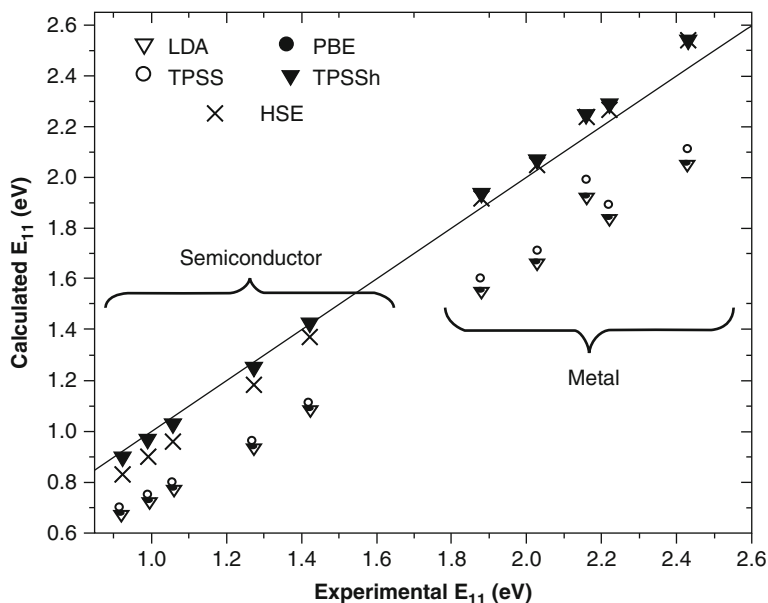
■ Fig. 24-5

Band structure (a) and optical spectrum (b) of the semiconducting (10,8) SWNT (Reprinted (Adapted) with permission from Barone et al. (2005b). © (2005) American Chemical Society)



■ Fig. 24-6

E_{11} mean errors in a set of ten semiconducting SWNTs calculated with different functionals



■ Fig. 24-7

Calculated versus experimental first optical excitation energies for semiconducting and metallic SWNTs (Reprinted (Adapted) with permission from Barone et al. (2005a). © (2005) American Chemical Society)

The success of the hybrid functionals HSE and TPSSh in predicting the peak position of optical transitions has been attributed to unknown error cancellations (Kümmel and Kronik 2008; Spataru et al. 2008). However, excitonic effects in metallic nanotubes are up to two orders of magnitude smaller than in semiconducting tubes (Deslippe et al. 2007) and remarkably, the same hybrid functionals that are able to describe the optical peaks in semiconducting tubes also produce excellent results in metallic tubes (Barone et al. 2005a).

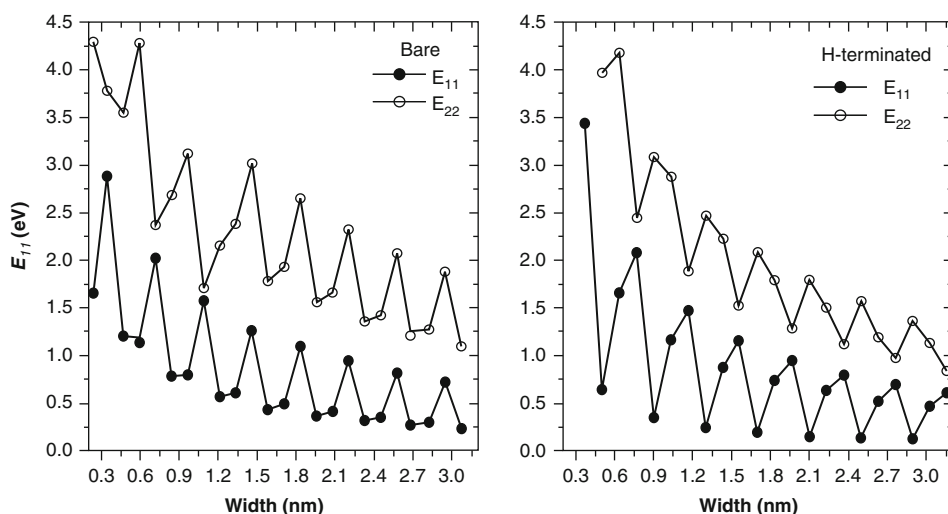
As a first example of the predictive capabilities of these functionals, we show in ● Fig. 24-7 calculated first-order optical transitions, E_{11} as a function of the corresponding experimental values in a set of five semiconducting and five metallic chiral nanotubes. All non-hybrid functionals employed here (LDA, PBE, and TPSS) underestimate E_{11} in metallic tubes by approximately 0.3 eV. This error is comparable to the error for E_{11} in semiconducting tubes. The best overall performance is achieved by the hybrids TPSSh and HSE, which yield comparable first-order transitions in the case of metallic SWNTs.

As a second example, we compare in ● Table 24-2 first-order transitions calculated using the hybrid TPSSh and HSE functionals (Barone et al. 2005a), and calculations considering GW plus electron-hole interactions (GW + e-h) (Spataru et al. 2008), with experimental values. Here, it is worth to point out the results obtained with hybrid functionals, that predict peak positions in agreement with more complex quasiparticle and excitonic effects approaches. An explanation for this behavior has been recently presented by Brothers et al. (2008).

■ Table 24-2

First-order optical transitions (eV) in metallic and semiconducting tubes calculated using the hybrid TPSSH and HSE functionals (Barone et al. 2005a, b), GW plus electron–hole interactions (GW + e–h) (Spataru et al. 2008), and experimental values

Tube	TPSSH	HSE	GW + e–h	Exp.	Reference (Exp.)
Semiconductor					
(10,0)	1.04	0.97	1.00	1.07	Bachilo et al. (2002)
(11,0)	1.19	1.12	1.21	1.20	Bachilo et al. (2002)
Metallic					
(12,0)	2.25	2.24	2.25	2.16	Fantini et al. (2004)
(10,10)	1.89	1.86	1.84	1.89	Fantini et al. (2004)



■ Fig. 24-8

Dependence of the first (E_{11}) and second (E_{22}) optical transition energies on the width of bare (*left panel*) and hydrogen-terminated (*right panel*) GNRs, at the HSE/6-31G* level of theory (Reprinted (Adapted) with permission from Barone et al. (2006). © (2006) American Chemical Society)

Graphene Nanoribbons

Theoretical and experimental studies reveal that the optical peaks of AGNRs might be utilized as tools to determine the nature of their edges (Barone et al. 2006; Pimenta et al. 2007). The first calculations of the optical spectrum of GNRs was presented by Barone et al. (2006) by means of DFT using the screened-exchange hybrid HSE functional. As expected from an inter-band transitions framework, first optical excitations present the corresponding oscillations as a function of the width. Second-order transitions also exhibit these oscillations, as shown in ● Fig. 24-8.

For armchair ribbons with hydrogen terminations there is a shift between the oscillation of the first and second optical transition energies such that the local maxima of E_{11} coincide with the local minima of E_{22} . This is expected to give rise to a doublet in the optical spectrum. A similar doublet is expected to appear for bare GNRs with widths smaller than 1.2 nm. Nevertheless,

for larger widths, the bandgap oscillations of the first and second optical transition energies of bare ribbons are in phase and the doublet is expected to disappear. This effect should provide a practical way of revealing information on the size and the nature of the edges of GNRs. Many-body approaches later pointed out that due to the one-dimensional nature of GNRs, and like in the case of SWNTs, their optical spectrum is dominated by excitonic effects with binding energies as high as 1.4 eV for a 1.2 nm wide ribbon (Prezzi et al. 2008; Yang et al. 2007).

Chemistry at the Edges of Graphene

The question of what is at the edges of graphene has fascinated researchers in the area (Radovic and Bockrath 2005), especially, since the possibility of finding magnetic edge states was openly discussed in terms of the type of chemical bond that is expected to appear for bare and hydrogen-terminated edges (Radovic and Bockrath 2005). The question of how magnetic and electronic properties of nanoribbons depend upon chemical functionalization and doping has been partially addressed by several studies. One of the first studies along this line of research was presented by Hod et al. (2007a). In this study, the authors assumed that in most synthetic scenarios GNRs edges will most likely be oxidized with an unknown effect on their electronic properties. The oxidation schemes considered in these calculations included hydroxyl, lactone, ketone, and ether groups. The authors have shown that these oxidized ribbons are, in general, more stable than hydrogen-terminated GNRs (see [Fig. 24-9](#)). These configurations maintain a spin-polarized ground state with antiferromagnetic ordering localized at the edges, similar to the fully hydrogenated counterparts. Edge oxidation has been found to lower the onset electric field required to induce half-metallic behavior (see [section “Graphene Nanoribbons”](#)) and extend the overall field range at which the systems remain half-metallic. When the edges of the ribbon are fully or partially hydrogenated, the field intensity needed to switch the system to the half-metallic regime is about 0.4 V/Å and the range at which the half-metallic behavior is maintained is of 0.3 V/Å. Nevertheless, when the edges are fully oxidized, the system turns half-metallic at a lower field intensity (0.2 V/Å) and the range of half-metallic behavior is doubled to 0.6 V/Å. Unfortunately, it is found that oxygen-containing groups at the edges have a minor effect on the energy difference between the antiferromagnetic ground state and the above-lying ferromagnetic state. This indicates a weak site-to-site exchange coupling and therefore oxygen terminations do not increase the spin coherence length in these systems.

Gunlycke et al. (2007) also studied the effect of oxygen and imine groups and found that transport and magnetic properties are greatly affected by the nature of the chemical groups at the edges. The electronic properties of ribbons with edge carbons presenting two hydrogen or two fluorine atoms were also studied and it was found that in narrow GNRs the sp^3 type of edge carbon results in a non-spin-polarized state (Kudin 2008). Kan et al. (2007) studied the effect of combining donor and acceptor groups at different edges of zigzag nanoribbons using DFT in the GGA. Within this approach, the authors found a half-metallic behavior without an external field for some particular chemical decorations. Cervantes-Sodi et al. (2008a, b) investigated the electronic properties of chemically modified ribbons and observed that chemical modifications of zigzag ribbons can lift the spin degeneracy which promotes a semiconducting-metal transition, or a half-semiconducting state, with the two spin channels having a different bandgap, or a spin-polarized half-semiconducting state, where the spins in the valence and conduction bands are oppositely polarized. The authors find that edge functionalization studied in

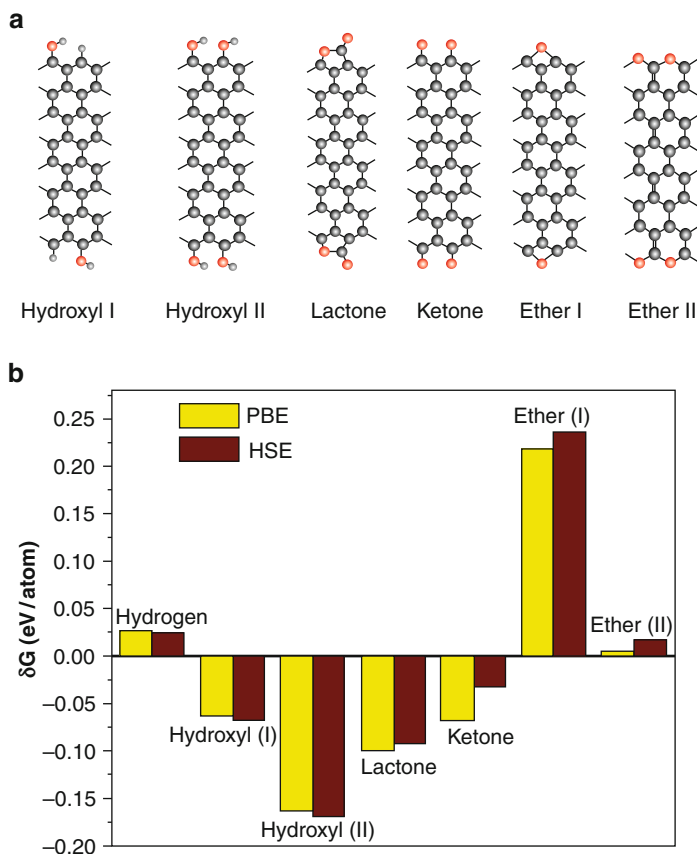


Fig. 24-9

(a) Scheme of the oxygen- containing groups considered. (b) Relative stability of the different chemical groups at the edges as calculated using the enthalpy of formation with respect to molecular oxygen and hydrogen, and graphene as shown in Hod et al. (2007a) (Reprinted (Adapted) with permission from Hod et al. (2007a). © (2007) American Chemical Society)

their work gives electronic states a few eV away from the Fermi level in armchair ribbons and does not significantly affect their bandgap. Lee and Cho (2009) presented calculations based on the local spin density approximation and found that edge-oxidated ZGNRs present a metallic behavior. This was rationalized in terms of the electronegativity of O with respect to C. However, it needs to be stressed that while LSDA or PBE calculations might yield a metallic solution, hybrid functionals still predict all oxidation schemes to be semiconducting (Hod et al. 2007a).

Chemical functionalization of rectangular graphene nanodots has been studied in detail using the DFT-B3LYP approach (Zheng and Duley 2008). This study shows that edge chemical modifications in finite ribbons significantly alter their electronic structure. Finite size effects in this type of dots will be further discussed in the next section.

It is interesting to note that besides chemical functionalization at the edges of graphene it is possible to introduce adatoms on the graphene surface. Usually, this type of interaction is

governed by a charge transfer mechanism. Rigo et al. (2009) presented DFT calculations on Ni adsorption on graphene nanoribbons. The adsorption takes place preferentially along the edges of zigzag nanoribbons and the interaction of the adatom with the carbon backbone quenches the magnetization of the latter in the neighborhood of the adsorption site. Other transition metal atoms adsorbed on GNRs were studied using DFT (Sevincli et al. 2008). Interestingly, Fe or Ti adsorption makes certain armchair GNRs half-metallic with a 100% spin polarization at the Fermi level. These results indicate that the properties of graphene nanoribbons can be strongly modified through the adsorption of 3d transition metal atoms. Alkaline and alkali metal adsorption on graphene nanoribbons were found to exhibit a strong site-dependent interaction (Choi and Jhi 2008). Similar results have been obtained by Uthaisar et al. (2009) when considering the interaction of Li adatoms and graphene nanoribbons. The strength of the interaction is much larger in zigzag GNRs than in armchairs and occurs preferentially along the edges. This enhancement is rationalized in terms of the larger number of electron acceptor states in ZGNRs compared to AGNRs. Energy barriers for Li migration also present important characteristics along the edges which can result in faster kinetics than in regular graphene (Uthaisar and Barone 2010). In addition, recent computational studies suggest lithium doping as a possible route for bandgap engineering of graphitic systems (Krepel and Hod 2011).

Finite Size Effects in Low-Dimensional Graphitic Materials

Finite size effects play a central role in dictating the electronic properties of materials at the nanoscale. Due to their unique electronic structure, quasi-zero-dimensional (quantum dots) graphitic structures may exhibit fascinating physical phenomena, which are absent in their quasi-one-dimensional (nanowires, nanotubes, and nanoribbons) counterparts. Many factors govern the effect of reduced dimensions on the electronic properties of nanoscale materials. Here we focus on two such important factors, which are strongly manifested in the electronic characteristics of graphitic materials, namely, quantum confinement and edge effects:

1. Quantum confinement is related to the boundary conditions enforced on the electronic wave function by the finite size of the system. When the typical de-Broglie wavelength associated with the Fermi electrons becomes comparable to the dimensions of the system, its electronic and optical properties deviate substantially from those of the bulk system. As the confining dimension decreases and reaches this limit (which is typically within the nanometer regime) the energy spectrum turns discrete and the energy gap becomes size dependent.
2. Edge effects in graphitic materials are dominated by localized states, which are physically located at the boundaries of the system and energetically positioned in the vicinity of the Fermi energy. These states influence not only the electronic properties of these systems but also their chemical reactivity.

Quantum Confinement in Graphitic Systems

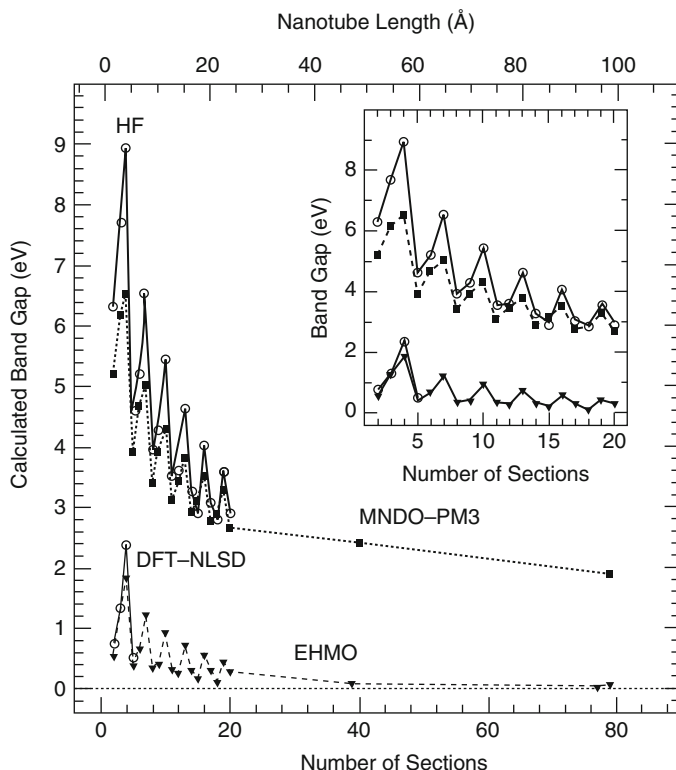
As shown in previous sections, combining the unique electronic structure of the two-dimensional graphene sheet with the quantum confinement in quasi-one-dimensional graphene derivatives, results in unique electronic properties, which are governed by the specific

geometry and dimensions of the relevant system. In [Section “Structure–Property Relations in Single-Walled Carbon Nanotubes and Graphene Nanoribbons,”](#) it was shown that one of the most notable examples of such effects is found in the strong dependence of the electronic character of carbon nanotubes on their specific diameter and chirality. This diversity in the electronic structure obtained from a single material just by changing its spatial symmetry, is one of the most promising characteristics of carbon nanotubes for applications as basic components in future nanoscale electronic devices.

Recent experimental procedures have allowed the production of ultra-short carbon nanotubes (Chen et al. [2006a, b](#); Gu et al. [2002](#); Javey et al. [2004](#); Khabashesku et al. [2002](#); Mickelson et al. [1998](#); Nakamura et al. [2003](#)). The electronic structure of these quasi-zero-dimensional systems is expected to be considerably different from their elongated counterparts, since the reduction of dimensionality implies additional confinement restrictions which may result in the emergence of new and interesting physical phenomena. Several theoretical investigations have addressed the importance of quantum confinement on the electronic properties of finite carbon nanotubes (Baldoni et al. [2007](#); Li et al. [2002](#); Liu et al. [2001](#); Rochefort et al. [1999b](#)). Using a variety of methods including the HF approximation, semiempirical calculations, and the GGA, Rochefort et al. ([1999b](#)) have investigated the change in bandgap, density of states, and binding energies as a function of the length of armchair carbon nanotubes. In contrast with the metallic character of the infinite tubes, finite segments shorter than 10 nm are predicted to present a considerable bandgap, which vanishes as the length of the tube increases. Interestingly, the convergence to the infinite metallic system is non-monotonic, and pronounced threefold bandgap oscillations occur as the length of the tube is extended (see [Fig. 24-10](#)). These bandgap oscillations were associated with the periodic changes in the bonding characteristics of the HOMO (highest occupied molecular orbital) and LUMO (lowest unoccupied molecular orbital), which are a direct consequence of the quantum confinement of the π electrons along the tube axis.

As one may expect, the calculated bandgaps strongly depend on the specific computational method, where the HF and semiempirical approximations predict bandgap values which are four to six times larger than those obtained by the generalized gradient DFT and extended Huckel calculations. Nevertheless, the general characteristics of the bandgap behavior and the existence of the bandgap oscillations are predicted by all methods. Similar results have been obtained using the hybrid B3LYP functional for open-ended and capped finite nanotube sections (Li et al. [2002](#)). Expanding the study to the case of zigzag and chiral nanotubes, Liu et al. ([2001](#)) have used extended Huckel calculations to show the dependence of the bandgap oscillations on the chirality of the finite nanotube segment. As shown in [Fig. 24-11](#), as the chirality of the tube changes gradually from armchair to zigzag, the amplitude of the oscillations reduces, and almost vanishes for the case of (12,0) zigzag nanotube segments. This leads to the interesting conclusion that the metallic character of the infinite armchair nanotubes is replaced by HOMO–LUMO gap oscillations for finite armchair nanotube segments, while the oscillatory bandgap nature of infinite zigzag nanotubes is replaced by a vanishing HOMO–LUMO gap for the finite zigzag nanotube segments. An interesting interpretation of the behavior of the HOMO and LUMO levels of finite carbon nanotube segments as a function of their length was recently given using Clar sextet theory (Baldoni et al. [2007](#)).

As discussed above, when an infinite graphene sheet is cut to form a quasi-one-dimensional graphene nanoribbon with a finite width and infinite length, the π -electrons wave function is confined along the direction perpendicular to the axis of the ribbon and is forced to vanish at large distances along this direction. These “particle in a box” like boundary conditions induce

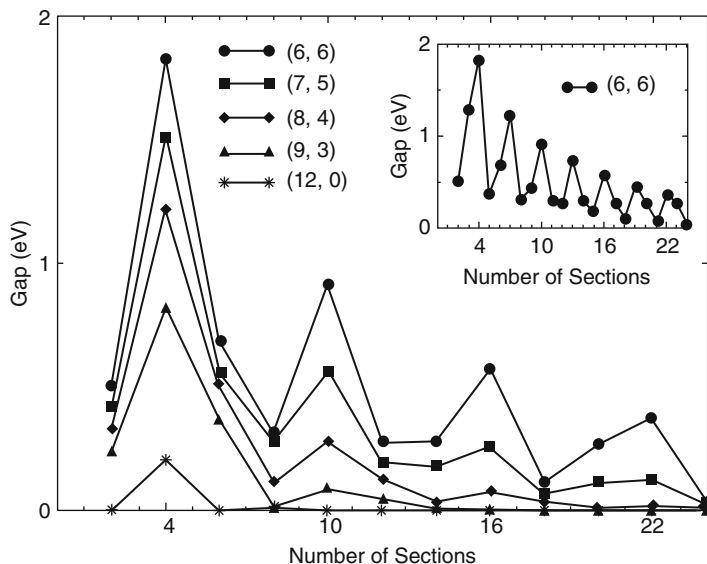


■ Fig. 24-10

Variation of the band gap of a (6,6) nanotube as a function of its length determined using different computational techniques (Reprinted (Adapted) with permission from Rochefort et al. (1999b). © (1999) American Chemical Society)

discretization of the two-dimensional dispersion relation into a set of one-dimensional bands. This discretization induces bandgap dependence on the width of the obtained ribbons.

The dimensionality of these systems may be further reduced to form graphene nanodots, which can be viewed as molecular derivatives of graphene. This extra confinement has been recently shown to strongly impact the electronic structure of these systems (Hod et al. 2008; Shemella et al. 2007). ● Figure 24-12 presents the HOMO-LUMO gaps as a function of the length and width of a large number of graphene quantum dots calculated using the local density approximation (upper left panel), the PBE flavor of the generalized gradient correction (upper right panel), and the screened-exchange hybrid HSE functional (lower left panel). The studied graphene derivatives are rectangular in shape and denoted by $N \times M$ where N and M are the number of hydrogen atoms passivating the armchair and zigzag edge, respectively. As in the case of infinite armchair graphene nanoribbons, an oscillatory behavior of the energy gap as a function of the length of the ribbon is observed. The periodicity of these oscillations appears to be somewhat different than the threefold period obtained for the infinitely long counterparts. This, however, is a result of the fact that in order to prevent dangling carbon bonds, the width step taken for the finite systems is twice as large than the one taken in the infinitely long armchair



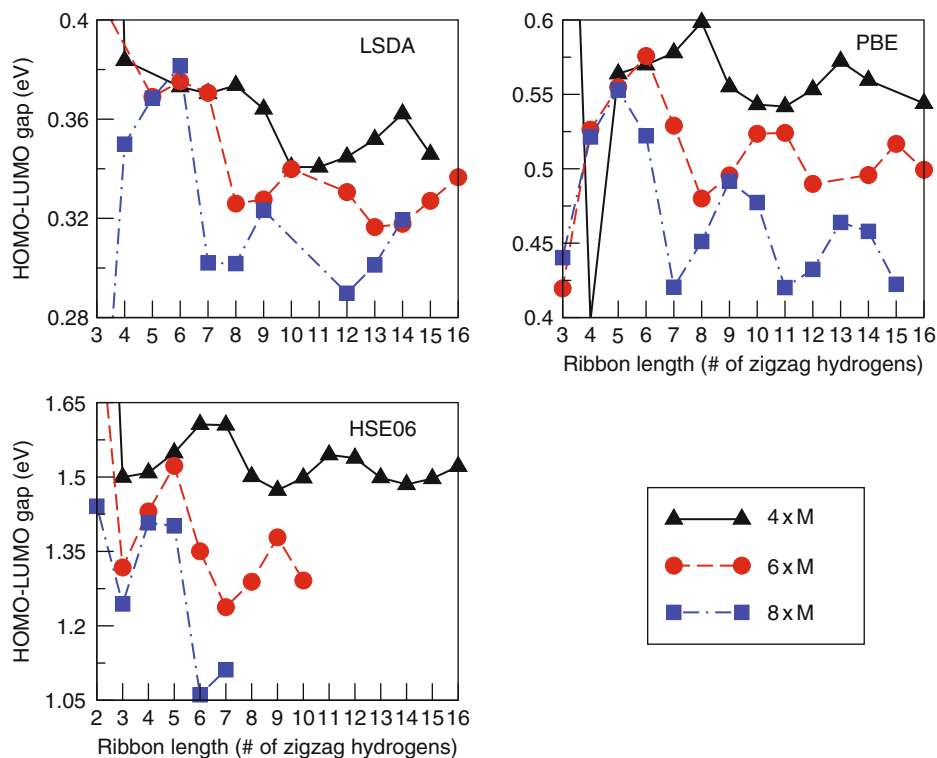
■ Fig. 24-11

The bandgap as a function of the (even) number of SWNTs sections (Reprinted with permission from Liu et al. (2001). © (2001) by the American Physical Society)

ribbon calculations. The amplitude of the oscillations is found to be considerably damped due to the finite size of the ribbons. As expected, when the length of the armchair edge (N) is increased, the oscillation amplitude increases as well. It is interesting to note that, in general, the HOMO–LUMO gap is inversely proportional to the width (N) and the length (M) of the finite GNR in accordance with the semimetallic graphene sheet limit. Therefore, in order to obtain energy gap tailoring capability, one will have to consider GNRs with long armchair edges (large N values) and short zigzag edges (small M values). This will increase the amplitude of the energy gap oscillations while maintaining overall higher gap values.

Edge Effects in Graphitic Systems

The effects of localized edge states on the electronic properties of quasi-one-dimensional systems have been discussed in previous sections. The question arises of whether similar effects can be observed in quasi-zero-dimensional systems. It is well established that small molecular derivatives of graphene, such as different types of polyaromatic hydrocarbons, have a closed shell nonmagnetic ground state. On the other hand, infinite ZGNRs present a spin-polarized ground state. This suggests that there exists a critical size at which molecular graphene derivatives become spin polarized. One of the earliest studies addressing this issue dates back to more than two decades ago (Stein and Brown 1987). Using Huckel theory it was found that finite graphene flakes exhibit electronic edge states along the zigzag edges. More recently, several studies, based on DFT calculations have investigated this question in detail. As a first step for obtaining quasi-zero-dimensional

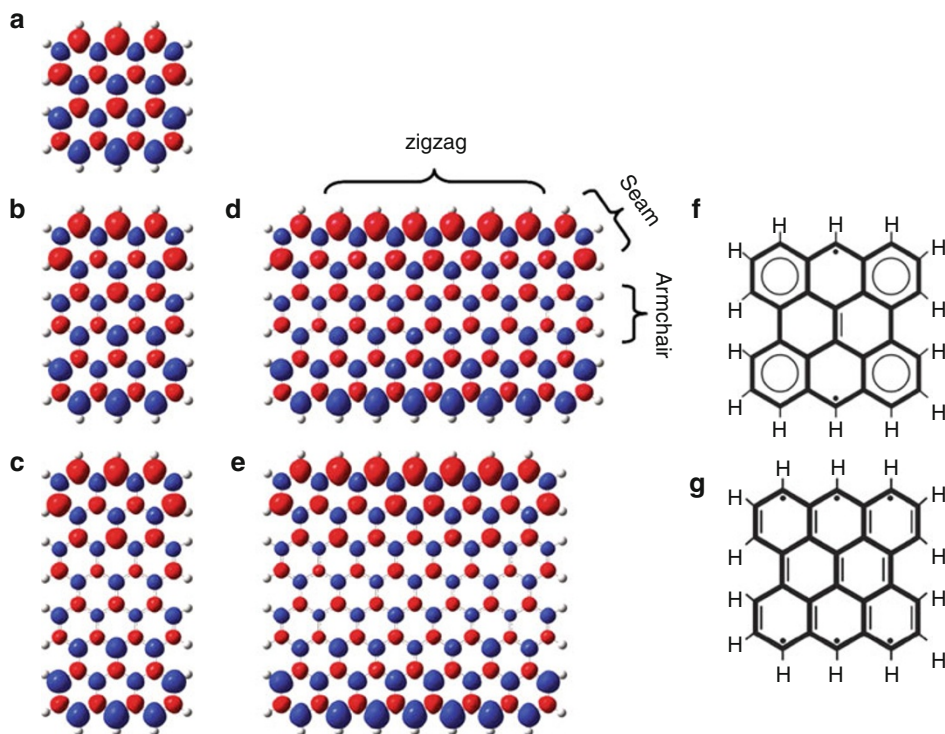


■ Fig. 24-12

HOMO–LUMO gap values for three sets of graphene nanodots, as calculated by the local spin density approximation (upper left panel), PBE functional (upper right panel), and the HSE functional (lower left panel) (Reprinted with permission from Hod et al. (2008). © (2008) by the American Physical Society)

graphene derivatives, it is convenient to consider truncated graphene nanoribbons in the form of rectangular nanodots (Hod et al. 2008; Jiang et al. 2007; Kan et al. 2007; Rudberg et al. 2007; Shemella et al. 2007). Surprisingly, it was found that even molecular scale graphene derivatives, such as the bisanthrene (phenanthro[1,10,9,8-opqra]perylene) isomer of the $C_{28}H_{14}$ molecule and $C_{36}H_{16}$ (tetrabenzo[bc,ef,kl,no]coronene), are predicted to present a spin polarized ground state as shown in ► Fig. 24-13 (Hod et al. 2008; Jiang et al. 2007; Kan et al. 2007). For the smaller molecules, this was further verified using a complete active space self-consistent field many-body-wave function approach (Jiang et al. 2007). Furthermore, the application of an in-plane electric field perpendicular to the zigzag edge was found to turn the finite systems into molecular scale half-metals (Hod et al. 2008; Kan et al. 2007), similar to the case of infinite ZGNRs.

When considering more complicated graphene derivatives such as triangular graphene flakes (Ezawa 2007; Fernandez-Rossier and Palacios 2007), the combination of the local anti-ferromagnetic spin ordering on adjacent carbon sites and the edge geometry of the triangular structure results in spin frustration. This leads to a metallic ground state with an overall ferromagnetic character and a finite magnetic moment. The results of tight-binding Ising model



■ Fig. 24-13

(a)–(e) Isosurface spin densities of the antiferromagnetic ground state of several molecular graphene derivatives as obtained using the HSE functional and the 6-31G** basis set. (f) and (g) represent diradical and hexaradical Clar structures of bisanthrene (Reprinted with permission from Hod et al. (2008). © (2008) by the American Physical Society)

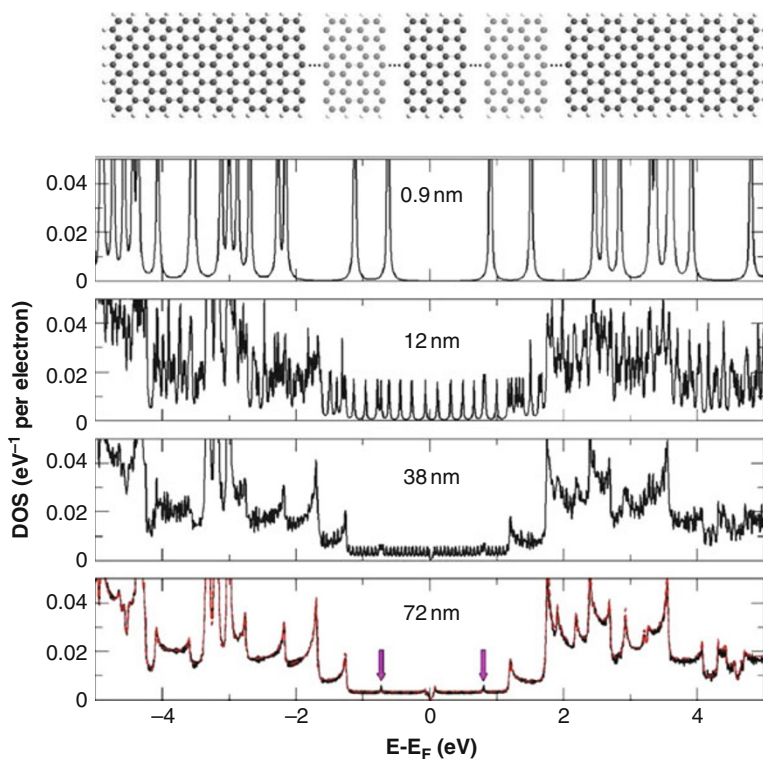
(Ezawa 2007) and Hubbard model (Fernandez-Rossier and Palacios 2007) Hamiltonians are consistent with the predictions of DFT (Fernandez-Rossier and Palacios 2007). These can be further rationalized by Lieb's theorem (Lieb 1989) regarding the total spin S of the exact ground state of the Hubbard model in bipartite lattices. The honeycomb lattice of graphene is formed by two triangular interpenetrating sublattices, A and B . Since triangular nanostructures have more atoms in one sublattice, $N_A > N_B$ the total spin S of the ground state is $2S = N_A - N_B > 0$. Here, the main contribution to the magnetic moment comes from edge states around the zigzag edges of the triangular structure. Such molecular graphene derivatives were suggested to function as permanent magnets in future nanoscale memory devices.

Naturally, the effect of edge states reduces as the surface to edge ratio becomes larger. An interesting question to address is at what length would the effect of the edges disappear and the electronic structure of the system becomes essentially identical to that of the infinite system? In a recent study, this question was addressed using a divide-and-conquer (D&C) DFT approach, which enables the efficient and accurate calculation of the electronic properties and charge transport through finite elongated systems (Hod et al. 2006). Within this approach, the Hamiltonian \mathbf{H} is given in a localized basis set representation by a block-tridiagonal matrix,

where the first and last diagonal blocks correspond to the two terminating units of the ribbon (see upper panel of [Fig. 24-14](#)). The remaining diagonal blocks correspond to the central part of the GNR which is composed of a replicated unit cell. The terminating units and the replicated central part unit cell are chosen to be long enough such that the block-tridiagonal representation of \mathbf{H} (and the overlap matrix \mathbf{S}) is valid. The terminating unit diagonal Hamiltonian blocks and their coupling to the central part are evaluated via a molecular calculation involving the two terminating units and one unit cell cut out of the central part. The replicated unit cell blocks of the central part and the coupling between two such adjacent blocks are approximated to be constant along the GNR and obtained from a periodic boundary conditions calculation. The resulting block-tridiagonal matrix $\mathbf{ES} - \mathbf{H}$ is then partially inverted for each value of the energy E using an efficient algorithm, to obtain the relevant Green's function blocks needed for the DOS and transport calculations using the following formula

$$\rho(E) = -\frac{1}{\pi} \text{Im} \{ \text{Tr} [G^r(E) \mathbf{S}] \}, \quad (24.2)$$

where $G^r(E) = [\mathbf{ES} - \mathbf{H}]^{-1}$. A detailed account of the D&C method can be found in Hod et al. (2006).

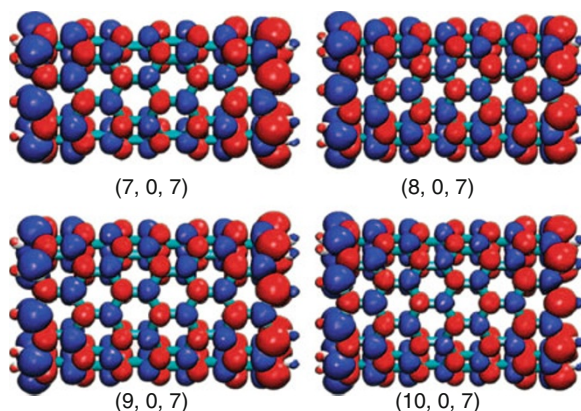


■ Fig. 24-14

Upper panel: A finite elongated graphene nanoribbon. **Lower panels:** DOS of the finite GNR at different lengths. The red curve in the lowermost panel is the DOS of the infinite system (Reprinted with permission from Hod et al. (2007b). © (2006) by the American Physical Society)

To study these edge effects in graphene, three graphene nanoribbons with consecutive widths were considered and their DOS as a function of the ribbons' length were calculated using this D&C approach (Hod et al. 2007b). As an example, [Fig. 24-14](#) presents the DOS of a finite graphene nanoribbon of different lengths. It can be seen that for graphene nanodots up to 12 nm in length, the DOS resembles that of a finite molecular system characterized by a discrete set of energy levels. When the ribbon is further elongated to 38 nm, a constant DOS around the Fermi energy of the infinite system arises and typical Van Hove singularities start to build up. For this specific system, at a length of 72 nm most of the features that are related to the edge states disappear, and the DOS almost perfectly matches that of an infinite armchair graphene nanoribbon. The rate of convergence of the electronic properties of finite systems to those of the infinite counterparts will depend on the type of the system and the specific interactions that govern its electronic character. Therefore, the divide-and-conquer method allows the quantitative estimation of this rate based on state-of-the-art DFT approximations.

We now turn back to the case of carbon nanotubes. When a zigzag nanotube is cut into finite segments, the zigzag edges are exposed. We have shown in the previous section that quantum confinement effects may play an important role in determining the electronic character of such structures. Similar to the case of graphene nanoribbons, these effects are now accompanied by the formation of spin-polarized edges states which put their own fingerprints on the electronic structures of the system (see [Fig. 24-15](#)). There has been a debate in the literature regarding the energetic stability of these edge states, and whether they would appear for all finite zigzag nanotubes regardless of their diameter (Higuchi et al. 2004; Kim et al. 2003; Okada and Oshiyama 2003). It is now well accepted that all finite zigzag SWNT segments are expected to present a spin-polarized ground state (Hod and Scuseria 2008; Kim et al. 2003; Mananes et al. 2008). Furthermore, as for ZGNRs, the application of an axial electric field will drive



■ Fig. 24-15

Antiferromagnetic-type ground state spin density maps of the (7,0) (*upper left panel*), (8,0) (*upper right panel*), (9,0) (*lower left panel*), (10,0) (*lower right panel*) finite zigzag SWNT segments as obtained using the HSE functional with the 6-31G** basis set. Red and blue isosurfaces indicate the two spin flavors with an isovalue of 0.0015 a_0^{-3} (Reprinted (Adapted) with permission from Hod and Scuseria (2008). © (2008) American Chemical Society)

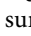
the system into a half-metallic state, thus forming a perfect spin filter. If one now eliminates only one zigzag edge of the tube by capping it with a half-fullerene, spin frustration results in a spin-polarized ferromagnetic ground state (Kim et al. 2003), which resembles the case of triangular graphene derivatives discussed above and forms a molecular magnet bearing a permanent magnetic moment.

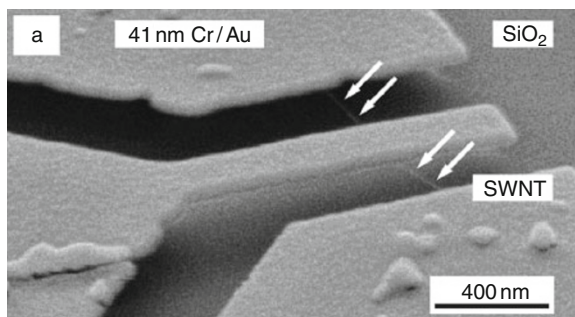
Two-dimensional graphene and its lower dimensional derivatives present a diversity of electronic behaviors, making them particularly attractive as building blocks for future nanodevices. Simplified model Hamiltonian approaches may give important insights on the general physical trends in these systems. Nevertheless, density functional theory in general, and the screen exchange hybrid functional approximation, in particular, seem to be excellent tools to quantitatively study the structure–function relations in these systems and the effects of external perturbations such as chemical substitutions and electric and magnetic fields.

Electromechanical Properties of One-Dimensional Graphitic Structures

Electromechanical devices are based on systems for which the mechanical properties can be controlled via the application of external electric potentials and/or the electronic properties may be altered via induced mechanical deformations. Such devices can be scaled down to form microelectromechanical systems (MEMS), which are small integrated devices or systems that combine electrical and mechanical components. Their dimensions may vary from the submicron level up to a few millimeters. By fabricating miniature mechanical elements such as beams, gears, diaphragms, and springs MEMS enabled the realization of diverse applications including ink-jet-printer cartridges, accelerometers, miniature robots, microengines, locks, inertial sensors, microtransmissions, micromirrors, micro actuators, optical scanners, fluid pumps, transducers, and chemical, pressure, and flow sensors. Nanoelectromechanical (NEMS) systems present the ultimate miniaturization of such devices, scaling them further down to the molecular level. Apart from the reduced dimensions, these systems are characterized by lower energy consumption and increased sensitivity toward external perturbations. Furthermore, due to their quantum-mechanical nature, molecular-sized NEMS may present unique physical properties that cannot be obtained from their microscopic and macroscopic counterparts. The unique electronic and mechanical properties of carbon nanotubes have marked them as promising candidates for key components in NEMS. In recent years, several theoretical investigations as well as experimental realization of NEMS have been presented (Cao et al. 2003; Cohen-Karni et al. 2006; Fennimore et al. 2003; Gomez-Navarro et al. 2004; Hall et al. 2007; Maiti 2003; Minot et al. 2003; Nagapriya et al. 2008; Paulson et al. 1999; Rueckes et al. 2000; Sazonova et al. 2004; Semet et al. 2005; Stampfer et al. 2006; Tomblor et al. 2000).

Carbon Nanotubes in NEMS Applications

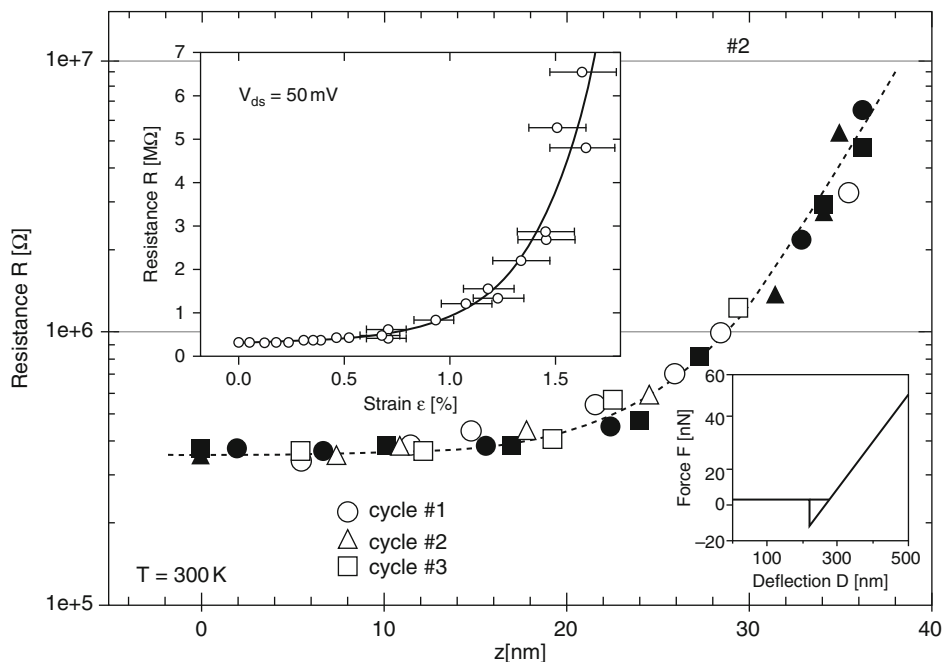
The key components in most of the suggested setups are suspended carbon nanotubes bridging the gap between two conducting electrodes without making contact with the underlying surface (see  Fig. 24-16). One may then induce mechanical deformations via manipulation of an external nanoscale tip while simultaneously measuring the changes in the conductance of



■ Fig. 24-16

SEM image of a cantilever-SWNT-based NEMS sensing device. The *white arrows* indicate the location of the suspended SWNT (Reprinted (Adapted) with permission from Stampfer et al. (2006). © (2006) American Chemical Society)

the system. Strong reversible electromechanical response of carbon nanotubes under combined bending and stretching deformations have been recorded by several experimental groups (Cao et al. 2003; Maiti 2003; Minot et al. 2003; Semet et al. 2005; Stampfer et al. 2006; Tombler et al. 2000). In ► Fig. 24-17, the change in the SWNT's resistance as a function of the depression applied to the top cantilever (► Fig. 24-16) is plotted. The resistance of the system increases by more than an order of magnitude over a depression range of less than 4 nm, suggesting that such setups may be used for highly sensitive and reliable displacement sensors. A similar setup, where a floating pedal is attached to a suspended multi-walled nanotube, has enabled the investigation of the electromechanical response of single (Hall et al. 2007) and multi-walled (Cohen-Karni et al. 2006) nanotubes under the application of torsional deformations. In this setup, an atomic force microscope (AFM) tip presses down on the floating pedal. Since the SWNT is fixed at both edges to the conducting electrodes, the central section experiences torsion. This change in helicity of the system induces considerable variations in the electronic conductance. Interestingly, pronounced bandgap oscillations are observed as a function of the deflection angle of the pedal. The origin of these oscillations has been associated with the distortion of the first Brillouin zone (fBZ), which results in the shifting of the Dirac points (Cohen-Karni et al. 2006; Nagapriya et al. 2008). As the Dirac points shift within the fBZ they may approach an allowed electronic band thus increasing the conductance of the system. Once the Dirac point crosses the allowed band the conductance reaches a maximum value. Further deformation results in shifting the Dirac points away from the allowed band and thus a decrease in the conductance. This process is repeated anytime the Dirac point crosses one of the many parallel allowed bands. Other prototype devices such as nanotube actuators (Fennimore et al. 2003; Gomez-Navarro et al. 2004), and nonvolatile memory components based on SWNTs junctions (Rueckes et al. 2000) have been successfully fabricated as well, demonstrating the potential of SWNTs as nanoscale electromechanical devices. Aiming to obtain a microscopic understanding of these experimental observations and to guide further experiments with carbon nanotubes under various mechanical deformation modes, many theoretical investigations have been performed (Maiti 2009). Due to the complexity of the deformed systems, most of the computational treatments were based on semiempirical or DFT-based TB calculations.



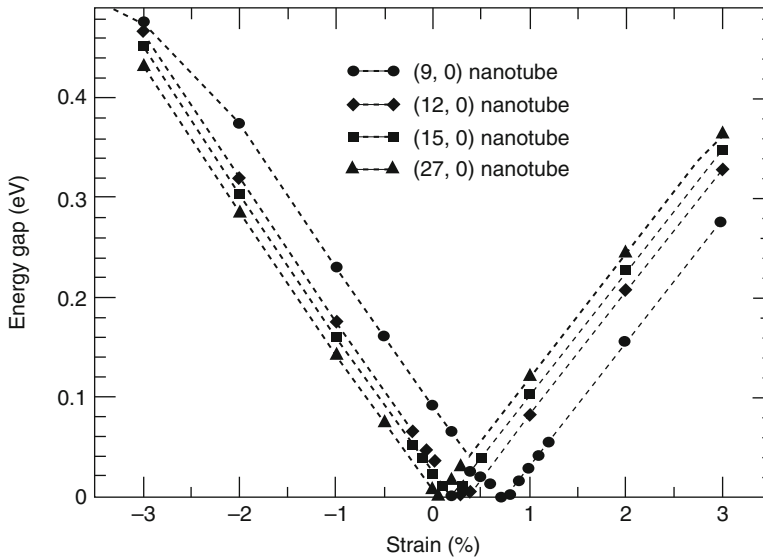
■ Fig. 24-17

Electromechanical measurements of an electromechanical device based on a metallic SWNT (► Fig. 24-16). The *upper insert* shows the resistance plotted as a function of strain. The *lower insert* shows a force versus deflection measurement performed on the cantilever-SWNT contact point (Reprinted (Adapted) with permission from Stampfer et al. (2006). © (2006) American Chemical Society)

The effects of axial stretching (Heyd et al. 1997; Jiang et al. 2004; Kane and Mele 1997; Kleiner and Eggert 2001; Yang et al. 1999), bending (Kane and Mele 1997; Liu et al. 2000; Nardelli 1999; Nardelli and Bernholc 1999; Rochefort et al. 1998, 1999a; Yang and Han 2000), torsion (Jiang et al. 2004; Kleiner and Eggert 2001; Rochefort et al. 1999a; Yang and Han 2000; Yang et al. 1999; Zhang et al. 2009), and radial compression (Lammert et al. 2000; Lu et al. 2003; Peng and Cho 2002; Svizhenko et al. 2005) were studied extensively showing high sensitivity of the electronic properties and transport characteristics of the deformed nanotubes to the applied deformations.

Several DFT calculations were conducted to study the effect of axial strain (Guo et al. 2005), bending (Maiti 2001; Maiti et al. 2002), radial compression (Mehrez et al. 2005; Wu et al. 2004), and torsional deformations in carbon nanotubes (Nagapriya et al. 2008):

1. *Axial strain*: While isolating the effect of axial stretching and compression is a challenging experimental task (Cao et al. 2003), pure axial deformations are easy to study using modern computational tools (Guo et al. 2005). Bandgap variations due to axial compression and stretching were studied using the local density approximation. As it can be seen in ► Fig. 24-18 for strains up to 3%, linear variations in the bandgap are predicted. The slope of the bandgap response depends on the tube type and on the sign of the axial deformation.



■ Fig. 24-18

Calculated bandgap variation of zigzag (9,0), (12,0), (15,0), and (27,0) SWNTs as a function of axial strain (Reprinted with permission from Guo et al. (2005). © (2005) American Institute of Physics)


For all systems studied, the relative changes in bandgap are of the order of 0.5 eV and are definitely measurable in experimental conditions.

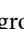
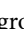
2. *Bending*: The effect of pure bending and AFM tip-induced bending was studied using the Harris functional approximation (Maiti 2001; Maiti et al. 2002). It was shown that both pure bending and tip-induced compression maintain the hexagonal sp^2 lattice structure up to relatively high bending angles. Armchair tubes remain significantly conducting even at large deformations. However, metallic zigzag tubes display a dramatic drop in conductance, in particular under tip-induced deformations.
3. *Compression*: Radial compression was studied via a combined molecular dynamics and density functional theory-based nonequilibrium Green's function approach (Wu et al. 2004). Reversible pressure-induced metal-to-semiconductor transitions of armchair SWNTs were predicted suggesting that SWNTs may be used as miniature sensitive pressure detectors (Mehrez et al. 2005; Wu et al. 2004).
4. *Torsion*: While the torsional electromechanical response was successfully explained via the deformation of the Brillouin zone, another possible explanation for the bandgap oscillations may be the periodic formation of Moire patterns due to registry mismatch between the different walls of the multi-walled tubes, which have a different curvature. In order to rule out this possibility, DFT calculations within the LSDA were used to show that the interlayer coupling is weak and the electronic structure of the individual walls resembles that of single-walled nanotubes for different intertube orientations (Nagapriya et al. 2008).

As can be seen from all of the examples given above, the study of the physical properties of nanotubes in general and their electromechanical behavior in particular requires

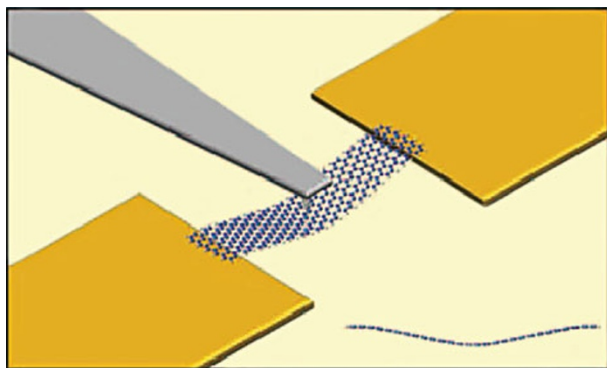
an intimate relation between theory and experiment, where the theoretical tools enable an atomic scale understanding of the experimental observations and provide guidelines for the design of new experiments. As we have seen above, when considering finite size effects and chemical functionalization, DFT presents new insights that are not captured within the simple TB approximations. When considering the electromechanical response of SWNTs to different mechanical deformations, TB calculations seem to give a reliable description. Nevertheless, calculations based on DFT are required for comparison and validation purposes.

Graphene Nanoribbons in NEMS Applications

Soon after the successful isolation of a single graphene sheet (Novoselov et al. 2004) the first experimental realization of an electromechanical device based on graphene nanoribbons was presented (Bunch et al. 2007). In this setup, atomic thick layers of graphene were suspended above predesigned trenches carved in the underlying silicon oxide surface while bridging the gap between gold electrodes. Both optical and electrical actuation procedures were demonstrated resulting in vibrational frequencies in the MHz regime. High charge sensitivities suggested the possibility of using similar devices as ultrasensitive mass and force detection (Bunch et al. 2007). Following this novel experimental fabrication and manipulation of graphene nanoribbons as nanoelectromechanical components, several other studies have explored the mechanical (Frank et al. 2007; Poot and van der Zant 2008) and electromechanical response of these systems (Milaninia et al. 2009). The effects of uniaxial strains in isolated graphene nanoribbons were recently studied in details using the generalized gradient approximation of the exchange correlation functional within the framework of DFT (Faccio et al. 2009; Sun et al. 2008). It was found that the electronic properties of zigzag GNRs are not sensitive to uniaxial strain, while the energy gap of armchair nanoribbons displays an oscillatory pattern as a function of the applied strain. By comparison to TB calculations, it was deduced that the nearest-neighbor hopping terms between atomic sites within the carbon hexagonal lattice are responsible for the observed electromechanical response. To simulate the effects of bending and torsional deformations in suspended graphene nanoribbons, DFT calculations utilizing the screened-exchange HSE density functional were performed (Hod and Scuseria 2009). A large set of short armchair graphene nanoribbons was considered, where narrow strips of atoms close to the zigzag edges of the ribbon were fixed to simulate a doubly clamped suspended nanoribbon (see  Fig. 24-19).

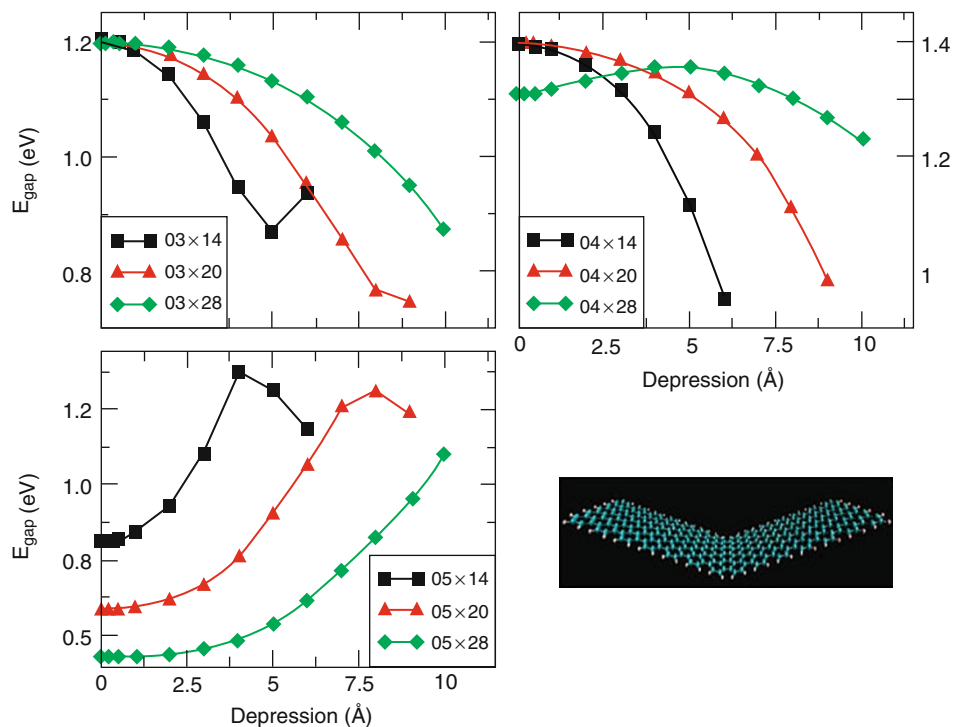
The effect of a driven deformation due to an external tip were simulated by constraining a strip of hexagons at the central part of the ribbon to be either depressed or rotated with respect to the fixed edge atoms. Extreme mechanical deformations, way beyond the linear response regime, were applied to the full set of nanoribbons studied. Most of the nanoribbons considered stayed stable under depressions of 1 nm as well as torsional angles of 90° maintaining their spin-polarized ground state character. As it can be seen in  Fig. 24-20, pronounced electromechanical responses for both bending and torsion (torsion not presented in  Fig. 24-20) have been obtained including evidence of dimension-dependent bandgap oscillations similar to the case of SWNTs (Cohen-Karni et al. 2006; Nagapriya et al. 2008).

Apart from indicating the promise that graphene nanoribbons hold from an electromechanical perspective, such calculations based on state-of-the-art density functional theory approaches, enhance the molecular scale understanding of the physical processes governing



■ Fig. 24-19

An artist view of an electromechanical device based on graphene nanoribbons. An external tip may induce bending and torsion of the nanoribbon (Reprinted (Adapted) with permission from Hod and Scuseria (2009). © (2009) American Chemical Society)



■ Fig. 24-20

HOMO-LUMO gap variations as a function of the depression applied to the central region of a doubly clamped GNR. Different panels and line colors represent results for GNRs of different widths and lengths, respectively (Reprinted (Adapted) with permission from Hod and Scuseria (2009). © (2009) American Chemical Society)

the behavior of these intriguing materials. Furthermore, theory and computations may guide future experiments to pursue promising scientific and technological routes toward which efforts and resources should be directed.

Concluding Remarks

In this chapter, we have given several examples of how theoretical investigations can be applied to elucidate the behavior of carbon nanostructures with emphasis on the understanding of the basic physical mechanisms that take place at the molecular level. In particular, we have shown that density functional theory is a powerful tool to this end, and we have provided several examples where density functional theory has been utilized to investigate electronic and structural properties of graphene nanoribbons, carbon nanotubes, and other low-dimensional graphitic materials. We hope that this chapter will furnish the reader with an ample background on this growing field and that it will serve as a starting point for readers interested in pursuing research in this exciting field.

Acknowledgments

VB acknowledges the donors of The American Chemical Society Petroleum Research Fund for support through the award ACS PRF#49427-UNI6. OH acknowledges the support of the Israel Science Foundation (Grant 1313/08), the Center for Nanoscience and Nanotechnology at Tel-Aviv University, the Lise Meitner-Minerva Center for Computational Quantum Chemistry, and the European Community's Seventh Framework Programme FP7/2007-2013 under grant agreement no. 249225. JEP acknowledges support from NSF DMR Award #DMR-0906617.

References

- Adamo, C., & Barone, V. (1999). Toward reliable density functional methods without adjustable parameters: The PBE0 model. *The Journal of Chemical Physics*, 110, 6158–6170.
- Adamson, R., Dombroski, J., & Gill, P. (1996). Chemistry without Coulomb tails. *Chemical Physics Letters*, 254, 329–336.
- Adamson, R., Dombroski, J., & Gill, P. (1999). Efficient calculation of short-range Coulomb energies. *Journal of Computational Chemistry*, 20, 921–927.
- Bachilo, S. M., Strano, M. S., Kittrell, C., Hauge, R. H., Smalley, R. E., & Weisman, R. B. (2002). Structure-assigned optical spectra of single-walled carbon nanotubes. *Science*, 298, 2361–2366.
- Balaban, A. T., & Klein, D. J. (2009). Claromatic carbon nanostructures. *Journal of Physical Chemistry C*, 113, 19123–19133.
- Baldoni, M., Sgamellotti, A., & Mercuri, F. (2007). Finite-length models of carbon nanotubes based on clar sextet theory. *Organic Letters*, 9, 4267–4270.
- Baldoni, M., Sgamellotti, A., & Mercuri, F. (2008). Electronic properties and stability of graphene nanoribbons: An interpretation based on Clar sextet theory. *Chemical Physics Letters*, 464, 202–207.
- Barone, V., & Scuseria, G. E. (2004). Theoretical study of the electronic properties of narrow single-walled carbon nanotubes: Beyond the local density approximation. *The Journal of Chemical Physics*, 121, 10376–10379.
- Barone, V., Peralta, J. E., & Scuseria, G. E. (2005a). Optical transitions in metallic single-walled carbon nanotubes. *Nano Letters*, 5, 1830–1833.
- Barone, V., Peralta, J. E., Wert, M., Heyd, J., & Scuseria, G. E. (2005b). Density functional theory

- study of optical transitions in semiconducting single-walled carbon nanotubes. *Nano Letters*, 5, 1621–1624.
- Barone, V., Hod, O., & Scuseria, G. E. (2006). Electronic structure and stability of semiconducting graphene nanoribbons. *Nano Letters*, 6, 2748–2754.
- Batista, E. R., Heyd, J., Hennig, R. G., Uberuaga, B. P., Martin, R. L., Scuseria, G. E., Umrigar, C. J., & Wilkins, J. W. (2006). Comparison of screened hybrid density functional theory to diffusion Monte Carlo in calculations of total energies of silicon phases and defects. *Physical Review B*, 74, 121102.
- Becke, A. D. (1993). Density-functional thermochemistry. III. The role of exact exchange. *The Journal of Chemical Physics*, 98, 5648–5652.
- Berger, C., Song, Z., Li, X., Wu, X., Brown, N., Naud, C., Mayou, D., Li, T., Hass, J., Marchenkov, A. N., Conrad, E. H., First, P. N., & de Heer, W. A. (2006). Electronic confinement and coherence in patterned epitaxial graphene. *Science*, 312, 1191.
- Bhardwaj, T., Antic, A., Pavan, B., Barone, V., & Fahlman, B. D. (2010). Enhanced electrochemical lithium storage by graphene nanoribbons. *Journal of the American Chemical Society*, 132, 12556–12559.
- Blase, X., Benedict, L. X., Shirley, E. L., & Louie, S. G. (1994). Hybridization effects and metallicity in small radius carbon nanotubes. *Physical Review Letters*, 72, 1878–1881.
- Brothers, E. N., Izmaylov, A. F., Normand, J. O., Barone, V., & Scuseria, G. E. (2008). Accurate solid-state band gaps via screened hybrid electronic structure calculations. *The Journal of Chemical Physics*, 129, 011102.
- Bunch, J. S., van der Zande, A. M., Verbridge, S. S., Frank, I. W., Tanenbaum, D. M., Parpia, J. M., Craighead, H. G., & McEuen, P. L. (2007). Electromechanical resonators from graphene sheets. *Science*, 315, 490–493.
- Cabria, I., Mintmire, J. W., & White, C. T. (2003). Metallic and semiconducting narrow carbon nanotubes. *Physical Review B*, 67, 121406.
- Cai, J., Ruffieux, P., Jaafar, R., Bieri, M., Braun, T., Blankenburg, S., Muoth, M., Seitsonen, A. P., Saleh, M., Feng, X., Müllen, K., & Fasel, R. (2010). Atomically precise bottom-up fabrication of graphene nanoribbons. *Nature*, 466, 470–473.
- Cao, J., Wang, Q., & Dai, H. (2003). Electromechanical properties of metallic, quasimetallic, and semiconducting carbon nanotubes under stretching. *Physical Review Letters*, 90, 157601.
- Cervantes-Sodi, F., Csányi, G., Piscanec, S., & Ferrari, A. C. (2008a). Edge-functionalized and substitutionally doped graphene nanoribbons: Electronic and spin properties. *Physical Review B*, 77, 165427.
- Cervantes-Sodi, F., Csányi, G., Piscanec, S., & Ferrari, A. C. (2008b). Electronic properties of chemically modified graphene ribbons. *Physica Status Solidi B*, 245, 2068–2071.
- Chen, Z., Kobashi, K., Rauwald, U., Booker, R., Fan, H., Hwang, W.-F., & Tour, J. M. (2006a). Soluble ultra-short single-walled carbon nanotubes. *Journal of the American Chemical Society*, 128, 10568–10571.
- Chen, Z., Ziegler, K., Shaver, J., Hauge, R., & Smalley, R. (2006b). Cutting of single-walled carbon nanotubes by ozonolysis. *Journal of Physical Chemistry B*, 110, 11624–11627.
- Chen, Z., Lin, Y.-M., Rooks, M. J., & Avouris, P. (2007). Graphene nano-ribbon electronics. *Physica E*, 40, 228–232.
- Choi, S.-M., & Jhi, S.-H. (2008). Self-assembled metal atom chains on graphene nanoribbons. *Physical Review Letters*, 101, 266105.
- Cohen-Karni, T., Segev, L., Srur-Lavi, O., Cohen, S. R., & Joselevich, E. (2006). Torsional electromechanical quantum oscillations in carbon nanotubes. *Nature Nanotechnology*, 1, 36–41.
- Deslippe, J., Spataru, C. D., Prendergast, D., & Louie, S. G. (2007). Bound excitons in metallic single-walled carbon nanotubes. *Nano Letters*, 7, 1626–1630.
- Ernzerhof, M., & Scuseria, G. E. (1999). Assessment of the Perdew-Burke-Ernzerhof exchange-correlation functional. *The Journal of Chemical Physics*, 110, 5029–5036.
- Ezawa, M. (2006). Peculiar width dependence of the electronic properties of carbon nanoribbons. *Physical Review B*, 73, 045432.
- Ezawa, M. (2007). Metallic graphene nanodisks: Electronic and magnetic properties. *Physical Review B*, 76, 245415.
- Faccio, R., Denis, P. A., Pardo, H., Goyenola, C., & Mombrú, A. W. (2009). Mechanical properties of graphene nanoribbons. *Journal of Physics Condensed Matter*, 21, 285304.
- Fantini, C., Jorio, A., Souza, M., Strano, M. S., Dresselhaus, M. S., & Pimenta, M. A. (2004). Optical transition energies for carbon nanotubes from resonant Raman spectroscopy: Environment and temperature effects. *Physical Review Letters*, 93, 147406.
- Feller, D. (1996). The role of databases in support of computational chemistry calculations. *Journal of Computational Chemistry*, 17, 1571–1586.

- Feller, D. (2007). *Basis set exchange: v1.2.2*. <https://bse.pnl.gov/bse/portal>.
- Fennimore, A., Yuzvinsky, T., Han, W., Fuhrer, M., Cumings, J., & Zettl, A. (2003). Rotational actuators based on carbon nanotubes. *Nature*, 424, 408–410.
- Fernandez-Rossier, J., & Palacios, J. J. (2007). Magnetism in graphene nanoislands. *Physical Review Letters*, 99, 177204.
- Frank, I. W., Tanenbaum, D. M., Van der Zande, A. M., & McEuen, P. L. (2007). Mechanical properties of suspended graphene sheets. *Journal of Vacuum Science & Technology B*, 25, 2558–2561.
- Frey, J. T., & Doren, D. J. (2005). *TubeGen Online - Version 3.3 - Web-Accessible nanotube structure generator*. <http://turin.nss.udel.edu/research/tubegenonline.html>.
- Frisch, M. J., Trucks, G. W., Schlegel, H. B., Scuseria, G. E., Robb, M. A., Cheeseman, J. R., Scalmani, G., Barone, V., Mennucci, B., Petersson, G. A., Nakatsuji, H., Caricato, M., Li, X., Hratchian, H. P., Izmaylov, A. F., Bloino, J., Zheng, G., Sonnenberg, J. L., Hada, M., Ehara, M., Toyota, K., Fukuda, R., Hasegawa, J., Ishida, M., Nakajima, T., Honda, Y., Kitao, O., Nakai, H., Vreven, T., Montgomery, Jr., J. A., Peralta, J. E., Ogliaro, F., Bearpark, M., Heyd, J. J., Brothers, E., Kudin, K. N., Staroverov, V. N., Kobayashi, R., Normand, J., Raghavachari, K., Rendell, A., Burant, J. C., Iyengar, S. S., Tomasi, J., Cossi, M., Rega, N., Millam, N. J., Klene, M., Knox, J. E., Cross, J. B., Bakken, V., Adamo, C., Jaramillo, J., Gomperts, R., Stratmann, R. E., Yazyev, O., Austin, A. J., Cammi, R., Pomelli, C., Ochterski, J. W., Martin, R. L., Morokuma, K., Zakrzewski, V. G., Voth, G. A., Salvador, P., Dannenberg, J. J., Dapprich, S., Daniels, A. D., Farkas, Ö., Foresman, J. B., Ortiz, J. V., Cioslowski, J., & Fox, D. J. (2006). *GAUSSIAN development version*, revision f.02. Wallingford CT: Gaussian Inc. 2009.
- Fujita, M., Wakabayashi, K., Nakada, K., & Kusakabe, K. (1996). Peculiar localized state at zigzag graphite edge. *Journal of the Physical Society of Japan*, 65, 1920–1923.
- Gomez-Navarro, C., de Pablo, P., & Gomez-Herrero, J. (2004). Radial electromechanical properties of carbon nanotubes. *Advanced Materials*, 16, 549.
- Gruneich, A., & Hess, B. (1998). Choosing GTO basis sets for periodic HF calculations. *Theoretical Chemistry Accounts*, 100, 253–263.
- Gu, Z., Peng, H., Hauge, R., Smalley, R., & Margrave, J. (2002). Cutting single-wall carbon nanotubes through fluorination. *Nano Letters*, 2, 1009–1013.
- Gülseren, O., Yildirim, T., & Ciraci, S. (2002). Systematic ab initio study of curvature effects in carbon nanotubes. *Physical Review B*, 65, 153405.
- Gunlycke, D., Li, J., Mintmire, J., & White, C. (2007). Altering low-bias transport in zigzag-edge graphene nanostrips with edge chemistry. *Applied Physics Letters*, 91, 112108.
- Guo, G., Liu, L., Chu, K., Jayanthi, C., & Wu, S. (2005). Electromechanical responses of single-walled carbon nanotubes: Interplay between the strain-induced energy-gap opening and the pinning of the Fermi level. *Journal of Applied Physics Letters*, 98, 044311.
- Hall, A. R., Falvo, M. R., Superfine, R., & Washburn, S. (2007). Electromechanical response of single-walled carbon nanotubes to torsional strain in a self-contained device. *Nature Nanotechnology*, 2, 413–416.
- Hamada, N., Sawada, S., & Oshiyama, A. (1992). New one-dimensional conductors – Graphitic microtubules. *Physical Review Letters*, 68, 1579.
- Han, M. Y., Oezylmaz, B., Zhang, Y., & Kim, P. (2007). Energy band-gap engineering of graphene nanoribbons. *Physical Review Letters*, 98, 206805.
- Heyd, J., & Scuseria, G. E. (2004). Efficient hybrid density functional calculations in solids: Assessment of the Heyd-Scuseria-Ernzerhof screened Coulomb hybrid functional. *The Journal of Chemical Physics*, 121, 1187–1192.
- Heyd, R., Charlier, A., & McRae, E. (1997). Uniaxial-stress effects on the electronic properties of carbon nanotubes. *Physical Review B*, 55(11), 6820–6824.
- Heyd, J., Scuseria, G. E., & Ernzerhof, M. (2003). Hybrid functionals based on a screened Coulomb potential. *The Journal of Chemical Physics*, 118, 8207–8215.
- Heyd, J., Peralta, J., Scuseria, G., & Martin, R. (2005). Energy band gaps and lattice parameters evaluated with the Heyd-Scuseria-Ernzerhof screened hybrid functional. *The Journal of Chemical Physics*, 123, 174101.
- Heyd, J., Scuseria, G. E., & Ernzerhof, M. (2006). Erratum: Hybrid functionals based on a screened Coulomb potential [*The Journal of Chemical Physics*, 118, 8207 (2003)]. *The Journal of Chemical Physics*, 124, 219906.
- Higuchi, Y., Kusakabe, K., Suzuki, N., Tsuneyuki, S., Yamauchi, J., Akagi, K., & Yoshimoto, Y. (2004). Nanotube-based molecular magnets with spin-polarized edge states. *Journal of Physics Condensed Matter*, 16, S5689–S5692.
- Hod, O., & Scuseria, G. E. (2008). Half-metallic-zigzag carbon nanotube dots. *ACS Nano*, 2, 2243–2249.
- Hod, O., & Scuseria, G. E. (2009). Electromechanical properties of suspended graphene nanoribbons. *Nano Letters*, 9, 2619–2622.

- Hod, O., Peralta, J. E., & Scuseria, G. E. (2006). First-principles electronic transport calculations in finite elongated systems: A divide and conquer approach. *The Journal of Chemical Physics*, 125, 114704.
- Hod, O., Barone, V., Peralta, J. E., & Scuseria, G. E. (2007a). Enhanced half-metallicity in edge-oxidized zigzag graphene nanoribbons. *Nano Letters*, 7, 2295–2299.
- Hod, O., Peralta, J. E., & Scuseria, G. E. (2007b). Edge effects in finite elongated graphene nanoribbons. *Physical Review B*, 76, 233401.
- Hod, O., Barone, V., & Scuseria, G. E. (2008). Half-metallic graphene nanodots: A comprehensive first-principles theoretical study. *Physical Review B*, 77, 035411.
- Iijima, S. (1991). Helical microtubules of graphitic carbon. *Nature*, 354, 58–56.
- Javey, A., Qi, P., Wang, Q., & Dai, H. (2004). Ten- to 50-nm-long quasi-ballistic carbon nanotube devices obtained without complex lithography. *Proceedings of the National Academy of Sciences of the United States of America*, 101, 13408–13410.
- Jiang, H., Bu, W., Jiang, J., & Dong, J. (2004). Electronic structure in finite-length deformed metallic carbon nanotubes. *The European Physical Journal B*, 42, 503–508.
- Jiang, D. E., Sumpter, B. G., & Dai, S. (2007). First principles study of magnetism in nanographenes. *The Journal of Chemical Physics*, 127, 124703.
- Kan, E. J., Li, Z., Yang, J., & Hou, J. G. (2007). Will zigzag graphene nanoribbon turn to half metal under electric field? *Applied Physics Letters*, 91, 243116.
- Kane, C. L., & Mele, E. J. (1997). Size, shape, and low energy electronic structure of carbon nanotubes. *Physical Review Letters*, 78(10), 1932–1935.
- Kataura, H., Kumazawa, Y., Maniwa, Y., Umez, I., Suzuki, S., Ohtsuka, Y., & Achiba, Y. (1999). Optical properties of single-wall carbon nanotubes. *Synthetic Metals*, 103, 2555–2558.
- Khabashesku, V., Billups, W., & Margrave, J. (2002). Fluorination of single-wall carbon nanotubes and subsequent derivatization reactions. *Accounts of Chemical Research*, 35, 1087–1095.
- Kim, Y., Choi, J., Chang, K., & Tomanek, D. (2003). Defective fullerenes and nanotubes as molecular magnets: An ab initio study. *Physical Review B*, 68, 125420.
- Klein, D. (1994). Graphitic polymer strips with edge states. *Chemical Physics Letters*, 217, 261–265.
- Kleiner, A., & Eggert, S. (2001). Band gaps of primary metallic carbon nanotubes. *Physical Review B*, 63(7), 073408.
- Kobayashi, K. (1993). Electronic-structure of a stepped graphite surface. *Physical Review B*, 48, 1757–1760.
- Kobayashi, Y., Fukui, K., Enoki, T., Kusakabe, K., & Kaburagi, Y. (2005). Observation of zigzag and armchair edges of graphite using scanning tunneling microscopy and spectroscopy. *Physical Review B*, 71, 193406.
- Kobayashi, Y., Fukui, K., Enoki, T., Kusakabe, K., & Kaburagi, Y. (2006). Edge state on hydrogen-terminated graphite edges investigated by scanning tunneling microscopy. *Physical Review B*, 73, 125415.
- Krepel, D., & Hod, O. (2011). Lithium adsorption on armchair graphene nanoribbons. *Surface Science*, 605, 1633–1642.
- Kroto, H., Heath, J., O'Brien, S., Curl, R., & Smalley, R. (1985). C-60 – Buckminsterfullerene. *Nature*, 318(6042), 162–163.
- Kudin, K. N. (2008). Zigzag graphene nanoribbons with saturated edges. *ACS Nano*, 2, 516–522.
- Kümmel, S., & Kronik, L. (2008). Orbital-dependent density functionals: Theory and applications. *Reviews of Modern Physics*, 80, 3–60.
- Kusakabe, K., & Maruyama, M. (2003). Magnetic nanographite. *Physical Review B*, 67, 092406.
- Lammert, P. E., Zhang, P., & Crespi, V. H. (2000). Gapping by squashing: Metal-insulator and insulator-metal transitions in collapsed carbon nanotubes. *Physical Review Letters*, 84(11), 2453–2456.
- Lee, G., & Cho, K. (2009). Electronic structures of zigzag graphene nanoribbons with edge hydrogenation and oxidation. *Physical Review B*, 79, 165440.
- Li, Z., Tang, Z., Liu, H., Wang, N., Chan, C., Saito, R., Okada, S., Li, G., Chen, J., Nagasawa, N., & Tsuda, S. (2001). Polarized absorption spectra of single-walled 4 angstrom carbon nanotubes aligned in channels of an AlPO₄₋₅ single crystal. *Physical Review Letters*, 87, 127401.
- Li, J., Zhang, Y., & Zhang, M. (2002). The electronic structure and its theoretical simulation of carbon nanotube with finite length. Part I: The frontier orbitals and its properties of short armchair nanotubes. *Chemical Physics Letters*, 364, 328–337.
- Lieb, E. (1989). 2 theorems on the Hubbard-model. *Physical Review Letters*, 62, 1201–1204.
- Liu, H. J., & Chan, C. T. (2002). Properties of 4 angstrom carbon nanotubes from first-principles calculations. *Physical Review B*, 66, 115416.
- Liu, L., Jayanthi, C. S., Tang, M., Wu, S. Y., Tomblor, T. W., Zhou, C., Alexseyev, L., Kong, J., & Dai, H. (2000). Controllable reversibility of an *sp*² to

- sp*³ transition of a single wall nanotube under the manipulation of an afm tip: A nanoscale electromechanical switch? *Physical Review Letters*, 84(21), 4950–4953.
- Liu, L., Jayanthi, C., Guo, H., & Wu, S. (2001). Broken symmetry, boundary conditions, and band-gap oscillations in finite single-wall carbon nanotubes. *Physical Review B*, 64, 033414.
- Lu, J.-Q., Wu, J., Duan, W., Liu, F., Zhu, B.-F., & Gu, B.-L. (2003). Metal-to-semiconductor transition in squashed armchair carbon nanotubes. *Physical Review Letters*, 90(15), 156601.
- Machón, M., Reich, S., Thomsen, C., Sánchez-Portal, D., & Ordejón, P. (2002). Ab initio calculations of the optical properties of 4-angstrom-diameter single-walled nanotubes. *Physical Review B*, 66, 155410.
- Maiti, A. (2001). Application of carbon nanotubes as electromechanical sensors – Results from first-principles simulations. *Physica Status Solidi*, 226, 87–93.
- Maiti, A. (2003). Carbon nanotubes – Bandgap engineering with strain. *Nature Materials*, 2, 440–442.
- Maiti, A. (2009). *Integrated analytical systems, computational methods for sensor material selection*. New York: Springer.
- Maiti, A., Svizhenko, A., & Anantram, M. (2002). Electronic transport through carbon nanotubes: Effects of structural deformation and tube chirality. *Physical Review Letters*, 88, 126805.
- Mananes, A., Duque, F., Ayuela, A., Lopez, M. J., & Alonso, J. A. (2008). Half-metallic finite zigzag single-walled carbon nanotubes from first principles. *Physical Review B*, 78, 035432.
- Mehrez, H., Svizhenko, A., Anantram, M., Elstner, M., & Frauenheim, T. (2005). Analysis of band-gap formation in squashed armchair carbon nanotubes. *Physical Review B*, 71, 155421.
- Mickelson, E., Huffman, C., Rinzler, A., Smalley, R., Hauge, R., & Margrave, J. (1998). Fluorination of single-wall carbon nanotubes. *Chemical Physics Letters*, 296, 188–194.
- Milaninia, K. M., Baldo, M. A., Reina, A., & Kong, J. (2009). All graphene electromechanical switch fabricated by chemical vapor deposition. *Applied Physics Letters*, 95, 183105.
- Minot, E., Yaish, Y., Sazonova, V., Park, J., Brink, M., & McEuen, P. (2003). Tuning carbon nanotube band gaps with strain. *Physical Review Letters*, 90, 156401.
- Mintmire, J., Dunlap, B., & White, C. (1992). Are fullerene tubules metallic? *Physical Review Letters*, 68, 631.
- Nagapriya, K. S., Berber, S., Cohen-Karni, T., Segev, L., Srur-Lavi, O., Tomanek, D., & Joselevich, E. (2008). Origin of torsion-induced conductance oscillations in carbon nanotubes. *Physical Review B*, 78, 165417.
- Nakada, K., Fujita, M., Dresselhaus, G., & Dresselhaus, M. S. (1996). Edge state in graphene ribbons: Nanometer size effect and edge shape dependence. *Physical Review B*, 54, 17954–17961.
- Nakamura, E., Tahara, K., Matsuo, Y., & Sawamura, M. (2003). Synthesis, structure, and aromaticity of a hoop-shaped cyclic benzenoid [10]cyclophenacene. *Journal of the American Chemical Society*, 125, 2834–2835.
- Nardelli, M. B. (1999). Electronic transport in extended systems: Application to carbon nanotubes. *Physical Review B*, 60(11), 7828–7833.
- Nardelli, M. B., & Bernholc, J. (1999). Mechanical deformations and coherent transport in carbon nanotubes. *Physical Review B*, 60(24), R16338–R16341.
- Niimi, Y., Matsui, T., Kambara, H., Tagami, K., Tsukada, M., & Fukuyama, H. (2005). Scanning tunneling microscopy and spectroscopy studies of graphite edges. *Applied Surface Science*, 241, 43–48.
- Novoselov, K. S., Geim, A. K., Morozov, S. V., Jiang, D., Zhang, Y., Dubonos, S. V., Grigorieva, I. V., & Firsov, A. A. (2004). Electric field effect in atomically thin carbon films. *Science*, 306, 666–669.
- Okada, S., & Oshiyama, A. (2003). Nanometer-scale ferromagnet: Carbon nanotubes with finite length. *Journal of the Physical Society of Japan*, 72, 1510–1515.
- Onida, G., Reining, L., & Rubio, A. (2002). Electronic excitations: Density-functional versus many-body Green's-function approaches. *Reviews of Modern Physics*, 74, 601–659.
- Paier, J., Marsman, M., & Kresse, G. (2007). Why does the B3LYP hybrid functional fail for metals? *The Journal of Chemical Physics*, 127, 024103.
- Paulson, S., Falvo, M., Snider, N., Helser, A., Hudson, T., Seeger, A., Taylor, R., Superfine, R., & Washburn, S. (1999). In situ resistance measurements of strained carbon nanotubes. *Applied Physics Letters*, 75, 2936–2938.
- Peng, S., & Cho, K. (2002). Nano electro mechanics of semiconducting carbon nanotube. *Journal of Applied Mechanics*, 69, 451.
- Peralta, J. E., Heyd, J., Scuseria, G. E., & Martin, R. L. (2006). Spin-orbit splittings and energy band gaps calculated with the Heyd-Scuseria-Ernzerhof screened hybrid functional. *Physical Review B*, 74, 073101.
- Perdew, J. P., Burke, K., & Ernzerhof, M. (1996). Generalized gradient approximation made simple. *Physical Review Letters*, 77, 3865–3868.

- Perdew, J. P., Ernzerhof, M., & Burke, K. (1997). Rationale for mixing exact exchange with density functional approximations. *The Journal of Chemical Physics*, 105, 9982–9985.
- Pimenta, M., Gomes, A., Fantini, C., Cancado, L., Araujo, P., Maciel, I., Santos, A., Furtado, C., Peressinotto, V., Plentz, F., & Jorio, A. (2007). Optical studies of carbon nanotubes and nanographites. *Physica E*, 37, 88–92.
- Poot, M. & van der Zant, H. S. J. (2008). Nanomechanical properties of few-layer graphene membranes. *Applied Physics Letters*, 92, 063111.
- Prezzi, D., Varsano, D., Ruini, A., Marini, A., & Molinari, E. (2008). Optical properties of graphene nanoribbons: The role of many-body effects. *Physical Review B*, 77, 041477.
- Radovic, L. R., & Bockrath, B. (2005). On the chemical nature of graphene edges: Origin of stability and potential for magnetism in carbon materials. *Journal of the American Chemical Society*, 127, 5917–5927.
- Reich, S., Thomsen, C., & Ordejón, P. (2002). Systematic ab initio study of curvature effects in carbon nanotubes. *Physical Review B*, 65, 153405.
- Rigo, V. A., Martins, T. B., da Silva, A. J. R., Fazzio, A., & Miwa, R. H. (2009). Electronic, structural, and transport properties of Ni-doped graphene nanoribbons. *Physical Review B*, 79, 075435.
- Ritter, K. A., & Lyding, J. W. (2009). The influence of edge structure on the electronic properties of graphene quantum dots and nanoribbons. *Nature Materials*, 8, 235–242.
- Rocheffort, A., Salahub, D. R., & Avouris, P. (1998). The effect of structural distortions on the electronic structure of carbon nanotubes. *Chemical Physics Letters*, 297, 45–50.
- Rocheffort, A., Avouris, P., Lesage, F., & Salahub, D. R. (1999a). Electrical and mechanical properties of distorted carbon nanotubes. *Physical Review B*, 60(19), 13824–13830.
- Rocheffort, A., Salahub, D., & Avouris, P. (1999b). Effects of finite length on the electronic structure of carbon nanotubes. *Journal of Physical Chemistry B*, 103, 641–646.
- Rudberg, E., Salek, P., & Luo, Y. (2007). Nonlocal exchange interaction removes half-metallicity in graphene nanoribbons. *Nano Letters*, 7, 2211–2213.
- Rueckes, T., Kim, K., Joselevich, E., Tseng, G., Cheung, C., & Lieber, C. (2000). Carbon nanotube-based nonvolatile random access memory for molecular computing. *Science*, 289, 94–97.
- Runge, E., & Gross, E. (1984). Density-functional theory for time-dependent systems. *Physical Review Letters*, 52, 997–1000.
- Saito, R., Fujita, M., Dresselhaus, G., & Dresselhaus, M. (1992). Electronic structure of graphene tubules based on C_{60} . *Physical Review B*, 46, 1804–1811.
- Saito, R., Dresselhaus, G., & Dresselhaus, M. S. (1998). *Physical properties of carbon nanotubes*. London: Imperial College Press.
- Sazonova, V., Yaish, Y., Ustunel, H., Roundy, D., Arias, T., & McEuen, P. (2004). A tunable carbon nanotube electromechanical oscillator. *Nature*, 431, 284–287.
- Semet, V., Binh, V., Guillot, D., Teo, K., Chhowalla, M., Amaratunga, G., Milne, W., Legagneux, P., & Pribat, D. (2005). Reversible electromechanical characteristics of individual multiwall carbon nanotubes. *Applied Physics Letters*, 87, 223103.
- Sevincli, H., Topsakal, M., Durgun, E., & Ciraci, S. (2008). Electronic and magnetic properties of 3d transition-metal atom adsorbed graphene and graphene nanoribbons. *Physical Review B*, 77, 195434.
- Sfeir, M. Y., Beetz, T., Wang, F., Huang, L. M., Huang, X. M. H., Huang, M. Y., Hone, J., O'Brien, S., Misewich, J. A., Heinz, T. F., Wu, L. J., Zhu, Y. M., & Brus, L. E. (2006). Optical spectroscopy of individual single-walled carbon nanotubes of defined chiral structure. *Science*, 312, 554–556.
- Shaver, J., Kono, J., Portugall, O., Krstic, V., Rikken, G. L. J. A., Miyauchi, Y., Maruyama, S., & Perebeinos, V. (2007). Magnetic brightening of carbon nanotube photoluminescence through symmetry breaking. *Nano Letters*, 7, 1851–1855.
- Shemella, P., Zhang, Y., Mailman, M., Ajayan, P. M., & Nayak, S. K. (2007). Energy gaps in zero-dimensional graphene nanoribbons. *Applied Physics Letters*, 91, 042101.
- Son, Y.-W., Cohen, M. L., & Louie, S. G. (2006a). Energy gaps in graphene nanoribbons. *Physical Review Letters*, 97, 216803.
- Son, Y.-W., Cohen, M. L., & Louie, S. G. (2006b). Half-metallic graphene nanoribbons. *Nature*, 444, 347–349.
- Spataru, C. D., Ismael-Beigi, S., Benedict, L. X., & Louie, S. G. (2004). Excitonic effects and optical spectra of single-walled carbon nanotubes. *Physical Review Letters*, 92, 077402.
- Spataru, C. D., Ismael-Beigi, S., Capaz, R. B., & Louie, S. G. (2008). Quasiparticle and excitonic effects in the optical response of nanotubes and nanoribbons. *Topics in Applied Physics*, 111, 195–227.
- Springborg, M., & Satpathy, S. (1994). Density-functional calculations of electronic and structural properties of small fullerene tubules. *Chemical Physics Letters*, 255, 454–461.

- Stampfer, C., Jungen, A., Linderman, R., Obergfell, D., Roth, S., & Hierold, C. (2006). Nano-electromechanical displacement sensing based on single-walled carbon nanotubes. *Nano Letters*, 6, 1449–1453.
- Stein, S., & Brown, R. (1987). Pi-electron properties of large condensed polyaromatic hydrocarbons. *Journal of the American Chemical Society*, 109, 3721–3729.
- Sun, L., Li, Q., Ren, H., Su, H., Shi, Q. W., & Yang, J. (2008). Strain effect on electronic structures of graphene nanoribbons: A first-principles study. *Journal of Chemical Physics*, 129, 074704.
- Svizhenko, A., Mehrez, H., Anantram, A. M. P., & Maiti, A. (2005). Sensing mechanical deformation in carbon nanotubes by electrical response: a computational study. *Proceedings of SPIE*, 5593, 416–428.
- Tanaka, K., Yamashita, S., Yamabe, H., & Yamabe, T. (1987). Electronic-properties of one-dimensional graphite family. *Synthetic Metals*, 17, 143–148.
- Tang, Z. K., Sun, H. D., Wang, J., Chen, J., & Li, G. (1998). Mono-sized single-wall carbon nanotubes formed in channels of AlPO_4 -5 single crystal. *Applied Physics Letters*, 73, 2287–2289.
- Tao, J., Perdew, J. P., Staroverov, V. N., & Scuseria, G. E. (2003). Climbing the density functional ladder: Nonempirical meta-generalized gradient approximation designed for molecules and solids. *Physical Review Letters*, 91, 146401.
- Telg, H., Maultzsch, J., Reich, S., Hennrich, F., & Thomsen, C. (2004). Chirality distribution and transition energies of carbon nanotubes. *Physical Review Letters*, 93, 177401.
- Tombler, T., Zhou, C., Alexseyev, L., Kong, J., Dai, H., Lei, L., Jayanthi, C., Tang, M., & Wu, S. (2000). Reversible electromechanical characteristics of carbon nanotubes under local-probe manipulation. *Nature*, 405, 769–772.
- Tsukada, M., Adachi, H., & Satoko, C. (1983). Theory of electronic-structure of oxide surfaces. *Progress in Surface Science*, 14, 113–173.
- Uthaisar, C., & Barone, V. (2010). Edge effects on the characteristics of Li diffusion in graphene. *Nano Letters*, 10, 2838–2842.
- Uthaisar, C., Barone, V., & Peralta, J. E. (2009). Lithium adsorption on zigzag graphene nanoribbons. *Journal of Applied Physics*, 106, 113715.
- Vanderbilt, D. (1990). Soft self-consistent pseudopotentials in a generalized eigenvalue formalism. *Physical Review B*, 41, 7892–7895.
- Vosko, S. H., Wilk, L., & Nusair, M. (1980). Accurate spin-dependent electron liquid correlation energies for local spin-density calculations – A critical analysis. *Canadian Journal of Physics*, 58, 1200–1211.
- Wakabayashi, K., Fujita, M., Ajiki, H., & Sigrist, M. (1999). Electronic and magnetic properties of nanographite ribbons. *Physical Review B*, 59, 8271–8282.
- Wang, F., Dukovic, G., Brus, L. E., & Heinz, T. F. (2005). The optical resonances in carbon nanotubes arise from excitons. *Science*, 308, 838–841.
- Wang, X., Ouyang, Y., Li, X., Wang, H., Guo, J., & Dai, H. (2008). Room-temperature all-semiconducting sub-10-nm graphene nanoribbon field-effect transistors. *Physical Review Letters*, 100, 206803.
- Wassmann, T., Seitsonen, A. P., Saitta, A. M., Lazzeri, M., & Mauri, F. (2008). Structure, stability, edge states, and aromaticity of graphene ribbons. *Physical Review Letters*, 101, 096402.
- Weisman, R. B., & Bachilo, S. M. (2003). *Nano Letters*, 3, 1235–1238.
- Wu, J., Zang, J., Larade, B., Guo, H., Gong, X., & Liu, F. (2004). Computational design of carbon nanotube electromechanical pressure sensors. *Physical Review B*, 69, 153406.
- Yang, L., & Han, J. (2000). Electronic structure of deformed carbon nanotubes. *Physical Review Letters*, 85(1), 154–157.
- Yang, L., Anantram, M. P., Han, J., & Lu, J. P. (1999). Band-gap change of carbon nanotubes: Effect of small uniaxial and torsional strain. *Physical Review B*, 60(19), 13874–13878.
- Yang, L., Cohen, M. L., & Louie, S. G. (2007). Excitonic effects in the optical spectra of graphene nanoribbons. *Nano Letters*, 10, 3112–3115.
- Yang, X., Dou, X., Rouhanipour, A., Zhi, L., Rader, H. J., & Müllen, K. (2008). Two-dimensional graphene nanoribbons. *Journal of the American Chemical Society*, 130, 4216.
- Zhang, D.-B., James, R. D., & Dumitrica, T. (2009). Electromechanical characterization of carbon nanotubes in torsion via symmetry adapted tight-binding objective molecular dynamics. *Physical Review B*, 80(11), 115418.
- Zhao, X., Liu, Y., Inoue, S., Suzuki, T., Jones, R. O., & Ando, Y. (2004). Smallest carbon nanotube is 3 angstrom in diameter. *Physical Review Letters*, 92, 125502.
- Zheng, H., & Duley, W. (2008). First-principles study of edge chemical modifications in graphene nanotubes. *Physical Review B*, 78, 045421.